Journal of Materials Chemistry A

Anti-Gas Hydrate Surfaces: Perspectives, Progress and Prospects

Journal:	*Journal of Materials Chemistry A*
Manuscript ID	TA-REV-10-2021-008965.R1
Article Type:	Review Article
Date Submitted by the Author:	21-Nov-2021
Complete List of Authors:	Wang, Feng; Norges teknisk-naturvitenskapelige universitet, Structural Engineering MA, Rui; Norwegian University of Science and Technology Xiao, Senbo; Norwegian University of Science and Technology, Department of Structural Engineering English, Niall; University College Dublin, School of Chemical + Bioprocess Engineering He, Jianying; Norwegian University of Science and Technology, Department of Structural Engineering; NTNU, Zhang, Zhiliang; Norwegian University of Science and Technology, Department of Structural Engineering

Anti-Gas Hydrate Surfaces: Perspectives, Progress and Prospects

Feng Wang[a], Rui Ma[a], Senbo Xiao[a,*], Niall J. English[b], Jianying He[a,*], Zhiliang Zhang[a,*].

a. NTNU Nanomechanical Lab, Department of Structural Engineering, Norwegian University of Science and Technology (NTNU), Trondheim 7491, Norway.

b. School of Chemical and Bioprocess Engineering, University College Dublin, Belfield, Dublin 4, Ireland

*E-mail: zhiliang.zhang@ntnu.no.

Abstract

Mitigating gas-hydrate formation and the subsequent gas-pipeline plugging is of critical importance for ensuring both flow assurance and safety in the exploration and transportation of deep-water resources. Until now, active methods that use chemicals and thermal energy are mainly applied in tackling the unwanted hydrate-accumulation problems. However, these methods not only are costly in and of themselves, but can also result in unavoidable environmental concerns. The rapid developments in surface-modification technology and advanced surface designs offer alternative solutions to mitigate the challenges raised by gas-hydrate formation. Newly-reported surfaces possess great potential for depressing gas-hydrate nucleation and deposition, and lowering hydrate adhesion, which has made passive anti-hydrate strategies possible. In this review, three current research priorities are pinpointed. Firstly, the intrinsic interactions between solid surface-gas hydrate should be scrutinized, which can shed light in solving the complex role of surface properties in hydrate nucleation. Secondly, hydrate-deposition mechanisms and surfaces that could suppress hydrate deposition need to be well understood, and, indeed, manipulated in their design. Of course, gas-hydrate deposition is more than a sequential process of hydrate agglomeration, and should be highly related to the underlying molecular chemistry/physics of surfaces. Thirdly,

hydrate adhesion from nano- to continuum-scales need to be correlated and understood well in terms of transition from one regime to the other; in such a way, this will facilitate the design of surfaces with low hydrate adhesion. After a thorough review on the fundamental relationships between surfaces and hydrate nucleation, deposition and adhesion, we shall discuss promising progress in gas-hydrate-inhibiting surfaces from the perspective of suppressing hydrate nucleation, inhibiting hydrate deposition and lowering hydrate adhesion, as well as gauging prospects for interesting directions in developing a comprehensive knowledge base for the design and creation of next-generation multifunctional hydrate-phobic surfaces.

Keywords**:** Gas hydrate, anti-hydrate surfaces, anti-hydrate nucleation, anti-hydrate deposition, anti-hydrate adhesion.

Introductions

Natural gas hydrates (hereinafter referred to as "hydrates") are water-based solids and ice-like crystals, which are formed by mixture of water and natural gas at high pressure and low temperature (typically 3-10 MPa at 0-10 °C)[1-3]. Hydrates have a crystalline, ice-like clathrate structure featuring a variety of cages which entrap caged natural gas (guest molecules)[4]. Three types of hydrate structures are observed in Nature, structure Ⅰ (sⅠ), structure Ⅱ (sⅡ) and structure H (sH)[2, 4, 5]. Specifically, sI represents a body-centered cubic structure that usually forms by small guest molecules (0.4-0.55 nm); sⅡ has a diamond lattice within a cubic framework which usually formed by large guest molecules (0.6-0.7 nm); and sH is a hexagonal framework contains both large and small guest molecules[5-8]. Large amounts of natural gas hydrates have been discovered in both the permafrost and marine-sediment, continental-shelf areas around the word[9-

[12]. The typical methane hydrate composition is usually represented as $(CH_4)_4(H_2O)_{23}$, which corresponds to 13.4 % methane in natural gas-hydrate by mass[13]. Because of the large volumetric storage potential in hydrate form, 1 m^3 of methane hydrate contains ~163 m^3 methane at 273 K under 1 atm, and hydrates hence represent an outstanding candidate as a future energy resource. The increasing interest in the research community on hydrates is also associated with far-reaching concerns on relevant sustainable technologies and gas-pipeline flow assurance[5, 14-17]. Because methane is an extremely potent greenhouse gas, its emission from natural reservoirs could greatly exacerbate global climate warming[18-20]. The ability to control hydrate formation and to manage hydrate stability is thus of great importance to various applications, including, *inter alia*, gas storage[21-24], gas separation[25-28], desalination[29-32], cold energy storage[33-36], and CO_2 capture and storage[37-44] - just to name a few pivotal areas.

Hydrates present great challenges to gas- and oil-production and transport systems. When water is present, gas hydrates can nucleate sequentially at gas-liquid interface, accumulate in flowline, deposit onto flowline walls, and block pipelines[45]. The undesired hydrate-plugs in pipelines restrict the gas/oil flow, resulting in over-pressurization and other catastrophic consequences. In the North Sea alone, there are ~7800 km of pipelines that can transport an amount of 96 billion cubic meters of gas per year[46]. With pressures spanning the range from 10 to 200 atm and seafloor temperature of 2-6 °C, hydrate-formation conditions are satisfied in large portions of such pipelines. Prevention of hydrate-plug formation and safe removal of hydrate-plugs are of great importance for deep-water flow assurance[47, 48]. State-of-the-art hydrate mitigation mainly rely on active methods by applying chemicals and inputting thermal energy. Generally, to suppress hydrate formation, thermodynamic inhibitors (THIs)[49-52] and kinetic hydrate inhibitors (KHIs)[53-56] are mostly used. Anti-agglomerates (AAs) are another option of commonly-used chemicals for preventing

aggregation of small hydrate crystals into large plugging masses[15, 57-59]. In the case when hydrate formation is inevitable, energy-intensive thermal techniques are also applied to dissolve hydrates[60-62]. Prevention of hydrate plugging and safe removal of hydrate plugs currently consume by far the most of deep-water flow-assurance efforts. According to a conservative estimation by Varanasi *et al.*, the costs associated with hydrate mitigation and with lost oil and gas production due to hydrate plugging can be billions of US dollars annually[63, 64]. Furthermore, these active methods are environmentally unfriendly. Therefore, alternative approaches that can reduce hydrate plugging through passive anti-hydrate surfaces design are in urgent demand[63].

There are three essential sequential stages identified in the formation of hydrate blockage in pipelines, namely 1) hydrate nucleation, growth and agglomeration, 2) hydrate deposition, and 3) hydrate plugging[45, 65, 66], as summarized in Fig. 1. Surfaces play critical roles in all the three stages of hydrate-blockage formation. In practice, the pipeline wall is the coldest component in the transport systems and provides intensive nucleation, deposition and adhesion sites for hydrate formation[67, 68]. As such, pipeline walls can significantly affect surface-based hydrate nucleation, growth and agglomeration. The physical/chemical states and properties of pipeline walls can also coordinate hydrate deposition, and determine the interfacial interaction and adhesion between deposited hydrates and wall surfaces. In this review, the published anti-gas hydrate surfaces are first categorized into three classes according to their functioning principles - namely anti-hydrate nucleation surfaces, anti-hydrate deposition surfaces and low hydrate adhesion surfaces, as shown in Fig. 1. Starting from the fundamental understanding of the three stages of hydrate blockage, followed by their interactions with surface properties, all three classes of anti-gas hydrate surfaces are thoroughly discussed. Perspectives and insights into the development of passive anti-gas hydrate surfaces are then offered, hinging on leveraging our underlying molecular-to-continuum

understanding of such processes for proposing cogent "molecular-assembly to continuum-programming" design rules – in the present case, with hydrate-nucleation/deposition/adhesion inhibition as the focus.

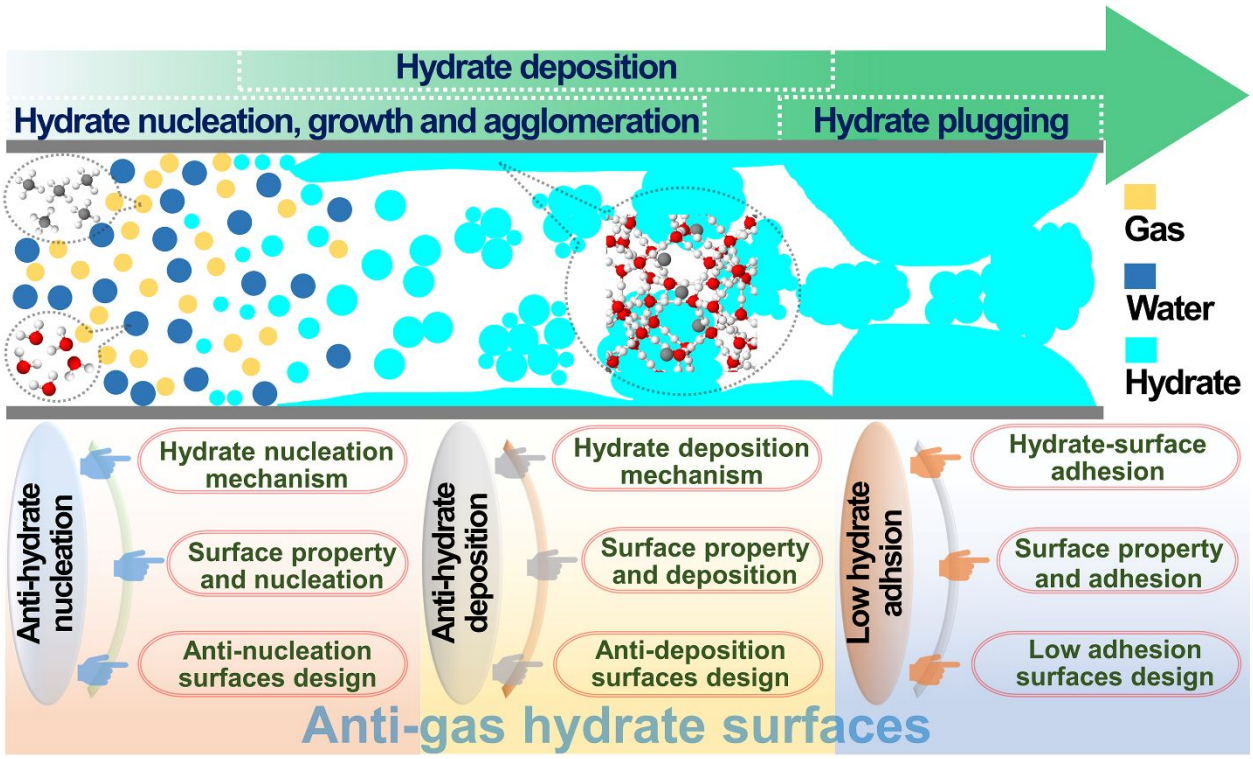

Figure 1. Gas-hydrate formation and anti-gas hydrate surfaces. The three stages of hydrate formation in pipelines are highlighted on the top panel, namely 1) hydrate nucleation, growth and agglomeration, 2) hydrate deposition, and 3) hydrate plugging. Anti-gas hydrate surfaces are classified into three categories based on the three stages of hydrate-blockage formation, namely anti-hydrate nucleation surfaces, anti-hydrate deposition surfaces, and low hydrate-adhesion surfaces, respectively. The fundamentals, properties and design strategies of each surface class are discussed in this work. The colors represent gas, water and hydrate are same applied in Figs. 5, 6 and 9.

1 Anti-hydrate nucleation surfaces

Theoretically, all hydrate-related phenomena are initiated from hydrate nucleation itself. Numerous efforts have focused on hydrate nucleation, from understanding nucleation mechanisms to hydrate nucleation promotion/inhibition. For mitigating the "hydrate-plugging" problem,

inhibiting hydrate nucleation is one of the most popular approaches. As a consequence, huge amounts of chemical agents (or inhibitors) that can thermodynamically/kinetically inhibit hydrate nucleation are used annually, which is costly and environmental hazardous[14, 15, 63]. Because hydrate nucleation is commonly observed at interfacial areas, including oil-gas interface, oil-water interface, solid surface, and so on[65], pipeline wall surfaces play essential roles in hydrate nucleation. Fabricating surfaces that can effectively inhibit hydrate nucleation is one of the appropriate choices for passive hydrate mitigation.

1.1 Hydrates' nucleation mechanism

It is crucial to firstly understand the basic mechanisms of hydrate nucleation, and then formulate strategies for inhibiting hydrate nucleation. Nucleation, either for hydrate or other crystalline structures, generally describes the initial process of generating solid from the liquid phase[69]. The structural and energy fluctuations in supercooled liquid may lead to a small, ordered molecular cluster in the disordered liquid phase. When the size of molecular cluster reaches the critical nucleus size, nucleation is followed by the subsequent rapid crystal growth process, leading to ordered structure propagation. The typical feature of crystal nucleation in the liquid phase is that the system needs to cross a free energy barrier. This process is widely described by the classical nucleation theory (CNT) proposed by Gibbs[70]. Crystal nucleation can be homogeneous or heterogeneous, according to different nucleation pathways. Therefore, hydrate nucleation mechanisms are discussed in the two distinct pathways.

1.1.1 Homogenous hydrate nucleation

Great efforts have been concentrating on revealing the homogeneous nucleation mechanism of hydrates starting in the early 1990s[71-74], which has yielded significant progress, especially in the last decade. The labile-cluster and local-structuring hypotheses (LCH & LSH, respectively) are two representative classical theories which attempt to explain homogenous nucleation of hydrates[71-73]. As the first attempt, the LCH proposed that the critical step of forming the nucleus of hydrate was the aggregation of isolated cage structures[71, 72]. In contrast, Radhakrishnan *et al.* found that the thermodynamically stable state of these cage structures should be mutually dispersed rather than aggregated, if multiple cage-like water molecular structures were formed in the liquid phase[73]. They then proposed the LSH, emphasizing that the guest molecules were first arranged to resemble their structure in hydrate followed by the surrounding water molecules evolved into a hydrate nucleus[73]. Later in 2010, Jacobsen *et al.* suggested that hydrate nucleation proceeded in two steps, namely the guest molecules and water molecules first formed a "blob" structure, and then this "blob" acted as a precursor to further induce the growth of amorphous cages that finally evolved into hydrate crystals (Fig. 2a)[75]. The stage of forming "blob" was a similar process as proposed in the LSH, that is the forming of clustered precursors by the aggregation of guest and water molecules. The subsequent aggregation and growth of "blob" feature the process proposed in LCH. Other recent studies supplied further understanding and more detailed explanations on the "blob" model[74, 76]. It's fair to say that the "blob" mechanism combines LSH and LCH, which lays the basis of much current understanding about homogeneous hydrate-nucleation mechanisms. It should be noted that the homogeneous hydrate nucleation hypotheses assume evenly mixed states of guest and water molecules, which could deviate from reality. As such, the probability of homogenous hydrate nucleation in a pipeline is low comparing to heterogeneous nucleation.

Certainly, reworkings of CNT have been carried out for hydrate nucleation to take into account residual thermodynamics for all phases, noting that many real hydrate systems, in both nature and industry, are rarely truly at thermodynamic equilibrium[77].

1.1.2 Heterogeneous hydrate nucleation

It is accepted that the free-energy barrier of heterogeneous nucleation is lower than homogeneous nucleation[70]. Heterogeneous hydrate nucleation is thus more probable in natural environments[78]. With a given gas-liquid interface in the system (usually caused by bubbles, whether macro- or micro-scopic), hydrates tend to nucleate and grow from the liquid side adjacent to the interface[79]. In such systems, locally high gas concentrations at the gas-liquid interface often trigger the nucleation of hydrates[79]. Furthermore, changes in the curvature of the gas-liquid interface influences the concentration of dissolved methane, and, subsequently, the rate of nucleation[80]. In gas-liquid-solid systems, nucleation of hydrates often starts from the three-phase contact area[81]. Preferential nucleation was observed around nano-bubbles adsorbed on solid surfaces in experiments[81, 82]; such results were consistent with CNT predictions. The nature of solid surface, via hydrate-surface interactions, can impact heterogeneous nucleation strongly. For instance, hydroxyl groups atop hydrophilic silica and clay surfaces could provide nucleation sites for the formation of hydrate cage structures[83-85]. On such surfaces, water cages and surface groups were observed to form a strong connection through hydrogen bonding (Fig. 2b). These strong hydrogen bonds can stabilize incipient hydrate crystals and promote hydrate formation[84]. In comparison, smooth and hydrophobic surfaces, such as the graphite family, lack surface functional groups for creating nucleation sites, which lead to ice-like water ordering observed near the

graphite surface (Fig. 2b). Such an ice-like structure was also able to promote gas hydrate formation compared to homogenous nucleation[84, 86].

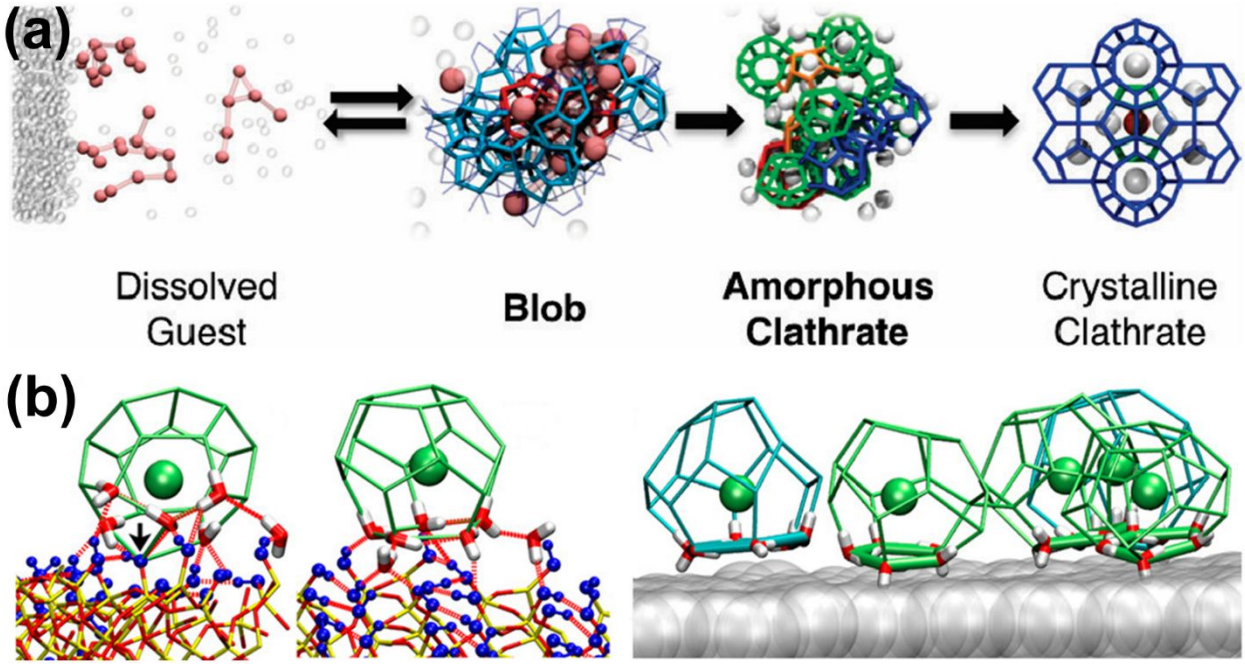

Figure 2. Homogeneous and heterogenous hydrate nucleation mechanism. (a) The homogenous "blob" hydrate nucleation, the guest molecules concentrated in "blob" first and then evaluated into hydrate crystal. (b) Heterogeneous hydrate nucleation: Contact modes of cages with the hydrophilic silica (left) and hydrophobic graphite (right) surfaces. Panel (a) was adapted with permission from Ref. 75, American Chemical Society. Panel (b) was adapted with permission from Ref. 84, American Chemical Society.

1.2 Surface properties and hydrate nucleation

As the difference in free-energy barrier discussed above, homogenous nucleation normally needs much longer time than that of heterogenous nucleation. Simulation results by Knott *et al.* have even indicated, perhaps unsurprisingly, that nucleation of methane hydrates under realistic conditions cannot be homogeneous[78]. Therefore, heterogeneous nucleation plays an - in fact, the - essential role in gas-hydrate formation in seafloor sediment, oil/gas transport pipelines, and, indeed, in high-pressure laboratory equipment. Although it has been suggested that heterogeneous hydrate

nucleation can be promoted by solid surfaces both thermodynamically and kinetically[87, 88], the corresponding mechanisms remain elusive and still need more exploration. Studies in identifying the functions of specific surfaces for impacting hydrate nucleation are important for probing the possible "anti-hydrate" properties of coatings with function of hydrate-nucleation inhibition.

1.2.1 Fundamentals of surface wettability

Surface wettability is critically important to hydrate formation and prevention. Generally, the wetting behavior of a surface is described by the tension components at the three-phase contact line of a droplet on the surface (Fig. 3a), i.e., the solid-liquid interfacial tension (γ_{SL}), the solid-vapor interfacial tension (γ_{SV}), and the liquid-vapor interfacial tension (γ_{LV}). The three tension components are correlated by the Young's equation (Eq. 1) proposed by Thomas Young[89]:

$$\gamma_{LV}\cos\theta = \gamma_{SV} - \gamma_{SL} \qquad (1)$$

where θ is the equilibrium contact angle of the liquid droplet on the flat solid surface. A solid surface is considered hydrophilic when a water droplet stays atop has contact angle $\theta < 90°$. Otherwise, the surface is hydrophobic (i.e. with water contact angle $\theta > 90°$). To account for the effects of roughness on the apparent contact angle of liquid on a solid surface, two models were developed by Wenzel[90] and Cassie and Baxter[91]. In the Wenzel model (Fig. 3b), surface roughness increases available surface area and modifies the surface contact angle following the equation:

$$\cos\theta^* = r\cos\theta \qquad (2)$$

where θ* is the apparent contact angle on the rough surface, r is the surface roughness factor that is defined by the ratio between actual and geometric surface area. In contrast, the Cassie-Baxter model (Eq. 3 and Fig. 3c) addresses microscopic pockets with trapped air on rough surfaces, and

introduces an new parameter f that represents the fraction of the solid in contact with the liquid droplet:

$$\cos\theta^* = -1 + f(1 + \cos\theta) \qquad (3)$$

The two new models thus describe to wetting states, namely the Wenzel and the Cassie-Baxter wetting states (Fig. 3c). Roughness can realize Cassie-Baxter state, allowing $\theta^* > 90°$ even with $\theta < 90°$. By introducing surface roughness, superhydrophobic surfaces ($150° < \theta^* < 180°$) can be achieved[92]. In the other extreme roughness also can enhance surface hydrophilicity, especially on flat surfaces with water contact angle $0° \leq \theta < 10°$, realizing the so-called superhydrophilicity. As such, four types of surface wetting behaviors, namely superhydrophilicity, hydrophilicity, hydrophobicity and superhydrophobicity can be observed on solid surfaces[93]. Since the surface wettability is highly related with surface chemistry, surface structure and environment, it thus can reflect the interactions between surfaces and water/hydrate droplets atop[92-94]. The surface wettability is a crucial parameter in the subsequent discussions regarding the relationship between surfaces and hydrate nucleation, deposition and adhesion.

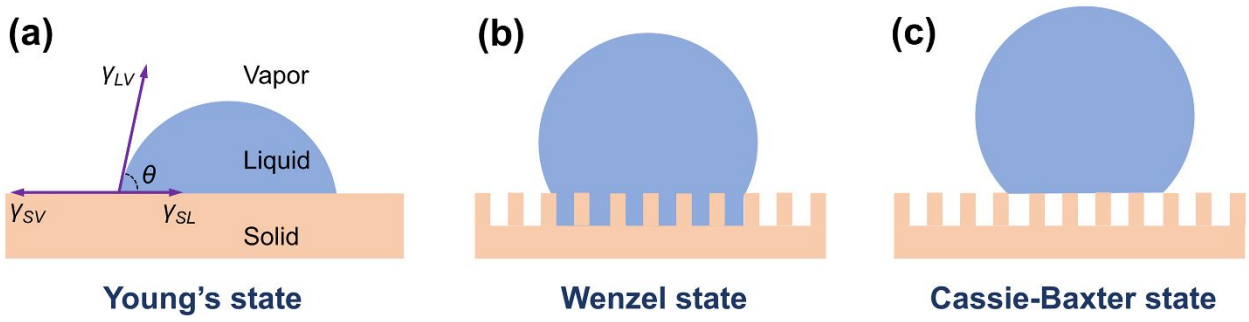

Figure 3. Surface wettability. (a) Young's state of a liquid droplet with an equilibrium contact angle θ on a smooth solid surface. The three important tension components at the three-phase contact line are indicated in the figure. Two wetting states of liquid droplets on rough surfaces: (b) the Wenzel and (c) the Cassie-Baxter state.

1.2.2 Surface chemistry and hydrate nucleation

Because of their intrinsically small length scales[45, 95], gas-hydrate nucleation *per se*, as opposed to more massive onset of hydrate formation after (stochastic) induction times have elapsed[77, 96], is generally notoriously challenging to study experimentally, but highly accessible by atomistic modeling and simulations. In natural conditions, silica, clay, or montmorillonite surfaces greatly influence hydrate formation in sediments[97-102]. Accordingly, many studies have focused on the heterogeneous clathrate-hydrate-nucleation behaviors on these surfaces[83, 88, 103-105]. Recently, Li *et al.* systematically studied the heterogenous nucleation behavior of methane hydrate in contact with kaolinite particles of various surface properties, including silica-alumina face, alumina-alumina face, and silica-silica face[106]. It was found that a siloxane surface was able to absorb methane molecules and assist formation of a semi-cage molecular arrangement at the siloxane-water interface. The semi-cage structure can serve as nucleation sites and promote methane-hydrate formation. In contrast, surfaces with hydroxyl groups hindered CH_4 molecules forming clathrate-like structures, owing to the strong hydrogen-bond interactions between the water and surface. As such, hydroxyl-rich surfaces did not necessarily promote gas-hydrate nucleation. Obviously, hydrate nucleation is significantly influenced by inherent surface-specific chemistry. Similarly, chemicals that absorbed/deposited on surfaces from flow phases also had clear effects on hydrate nucleation. In oil/gas-transportation systems, metal pipe walls are most probable to be covered with water or oil, which are essential for the nucleation of gas hydrate[107]. In this vein, Zi *et al.* have investigated various types of gas-hydrate nucleation behavior on rough metal surfaces covered with water, light oil (toluene), and heavy oil (asphaltene + toluene) using molecular-dynamics simulation[104]. Their results showed that light oil on metal surfaces effectively inhibited gas hydrate growth, and heavy oil further enhanced this inhibition effect. Other experimental results also

demonstrated that surfactants, oxygen-containing surface functional groups, and polyol coatings could influence hydrate formation, although nucleation was hard to be identified in experiments[103, 108, 109]. These results clearly suggest that surface with variable chemistries can be utilized for modulate hydrate nucleation.

A further important point, which is relevant for both home- and heterogeneous hydrate formation, is that the transport delayed of gas molecules' transport (possibly as macro- or microscopic bubbles) by hydrate films themselves present formidable barriers that serves to slow down contact and reduce scope for further hydrate growth and depositions[77]. Of course, as we shall see (*vide infra*), surface chemistry also affects - indeed, controls - this level of hydrate-film deposition at surfaces. In any event, experimentally, the gas-transport delay this is often manifested as a greater induction times, or time delay for onset of massive growth, although other mass-transport delays of gas through the liquid phase can also reflect this experimentally-observable statistically-distributed induction times[110].

1.2.3 Surface hydrophobicity and hydrate nucleation

To explore the relationship between surface hydrophobicity and hydrate nucleation, He *et al.* investigated methane-hydrate formation on hydrophilic silica and hydrophobic graphite surfaces[84]. Their results indicated that different surface hydrophobicity indeed resulted in distinct hydrate nucleation behaviors. The graphite surface absorbed methane molecules and formed a nanobubble with a flat/negative curvature, leading to low solvated methane concentration and long waiting time of hydrate nucleation of more than 2.5 μs in simulations. On the contrary, the hydrophilic silica surface favored water molecules and left a high solvated methane concentration in the bulk, which significantly promoted a high hydrate nucleation rate. Similarly, for biological surfaces

(proteins and particularly favorable peptide sequences), Ghaani and co-workers have studied with acuity, using both experimental and molecular-simulation approaches, the interplay of hydrophobic and hydrophilic sequences of amino-acid residue sequences for methane-hydrate formation thereon, including the effect of chirality and magnetic fields[111-113]. It was found, broadly, that judicious selection of alternating hydrophobic/hydrophilic surfaces allow for the optimal "scaffolding" to promote methane-hydrate formation, and general establishment "molecular-surface engineering" design principles and rules are of course important if one wishes to regulate and manipulate surface-based hydrate formation (whether inhibition or promotion, although the present review focuses, naturally, on inhibition).

Other studies have also showed, rightly, that gas concentration, and especially local supersaturation, is a critical factor governing hydrate nucleation[79, 80]. As shown in Fig. 4a, the mole fraction of CH_4 in water (X_{CH4}) and order parameter F_4 (which described torsion angle between the oxygen atoms of two water molecules within 0.35 nm and the outermost hydrogen atoms) were used to track and identify hydrate nucleation. Importantly, albeit perhaps not so unsurprisingly, as X_{CH4} was kept low, hydrate nucleation was not observed in systems with graphite surfaces, but when a bulk-hydrate-like X_{CH4} was present (in the local liquid phase, about 30-40 times supersaturated from a Henry's-Law perspective) in the case of silica systems, nucleation occurred very readily[84]. Sarupria *et al.* have utilized self-assembled monolayers (SAMs) that terminated with different chemical groups to modify surface hydrophobicity, and studied their effects on hydrate nucleation[114]. In their work, -OH terminated self-assembled monolayers (OHSAM) and -CH_3 terminated self-assembled monolayers (CH_3SAM) were taken as models of hydrophilic and hydrophobic surfaces, respectively. Nucleation was initiated more quickly in OHSAM systems compared to CH_3SAM systems, as indicated by Fig. 4b. The presence of -OH groups on the SAM

surface caused higher bulk gas supersaturation concentration in OHSAM systems and higher nucleation rate.

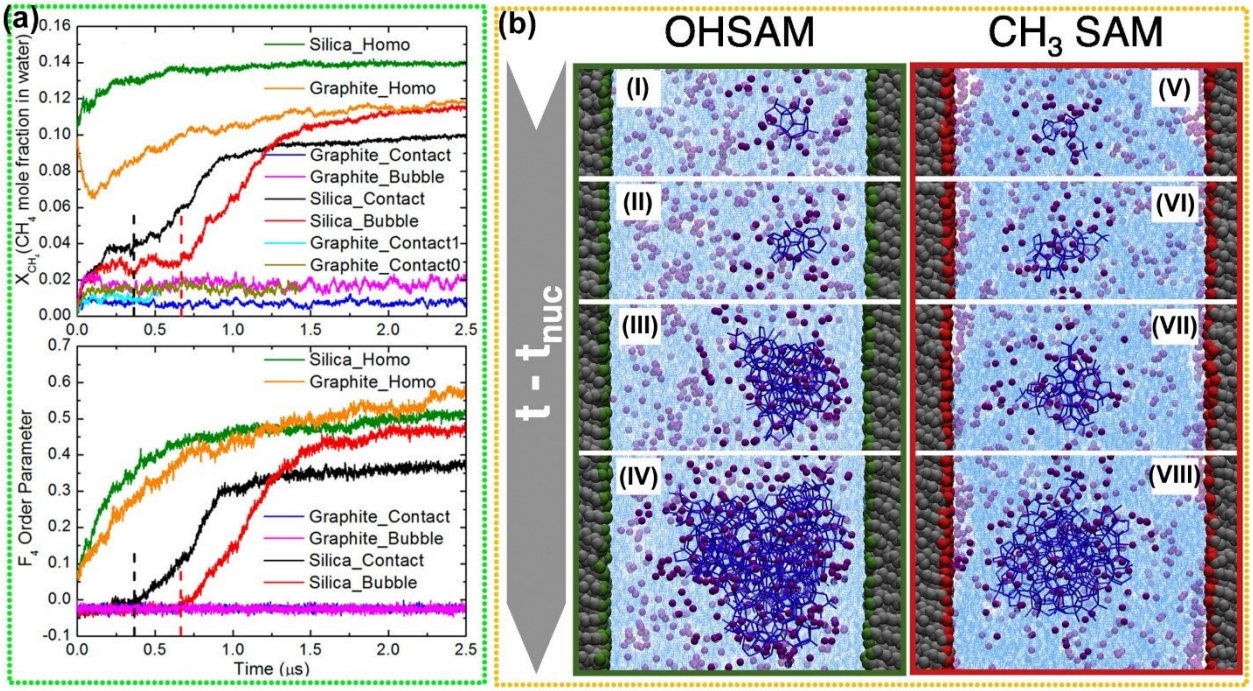

Figure 4. Surface hydrophobicity and hydrate nucleation. (a) Hydrate nucleation behavior on graphite and silica surfaces. X_{CH4} and F_4, mole fraction and order parameter respectively, in various graphite and silica systems during 2.5 μs simulations. The black and red dash lines indicated nucleation events via Silica_Contact and Silica_Bubble, respectively. (b) Snapshots of hydrate nucleation behaviors on hydrophilic OHSAM (Ⅰ ~ Ⅳ) and hydrophobic CH_3SAM (Ⅴ ~ Ⅷ) systems at 233 K. Panel (a) was adapted with permission from Ref. 84, American Chemical Society. Panel (b) was adapted with permission from Ref. 114, Elsevier Publishing Group.

1.2.4 Surface porous structure and hydrate nucleation

It has been widely observed both in natural and experimental conditions that porous materials can intensify hydrate formation[115-117]. Unfortunately, direct observation of crystal nucleation of hydrate in porous structures in experiments remains a highly challenging task. However, by employing molecular-dynamics simulation, hydrate nucleation behaviors on surfaces with

nanopores were investigated[83, 85, 104]. Wu *et al.* studied the influence of surface porous structures on methane-hydrate nucleation[104]. As shown in Fig. 5, the results indicate that rough surfaces can kinetically promote hydrate nucleation thanks to the altered methane concentration inside surface grooves. As shown by the methane concentration monitored at different regions of surfaces in Fig. 5, the solvated methane at the upper part of the grooves increased by 45% in the first 120 ns of simulation time. Hydrate nucleation was also more likely to start from the upper part of the grooves. It should be noted that the preferable trend of hydrate nucleation can be changed when oil was present on surfaces. Based on the simulation results, Wu *et al.* speculated that corrosion of carbon steel in practical pipe walls could greatly facilitate hydrate nucleation, and this has also been suggested and observed by Kvamme *et al.*[118, 119]. Interestingly, it was confirmed that changes in the physical structures (pores and grooves) had more significant effects than changes in the chemical properties (formation of rust) in promoting hydrate formation[120]. Yan *et al.* studied the hydrate nucleation and growth process in a system contain clay surfaces with nanopores[83]. They found that hydrate formation in porous media was much more complex than in the bulk solution, which involved cooperativity between hydrate growth and molecular diffusion[83]. Therefore, pore size is also a key parameter which affects hydrate formation.

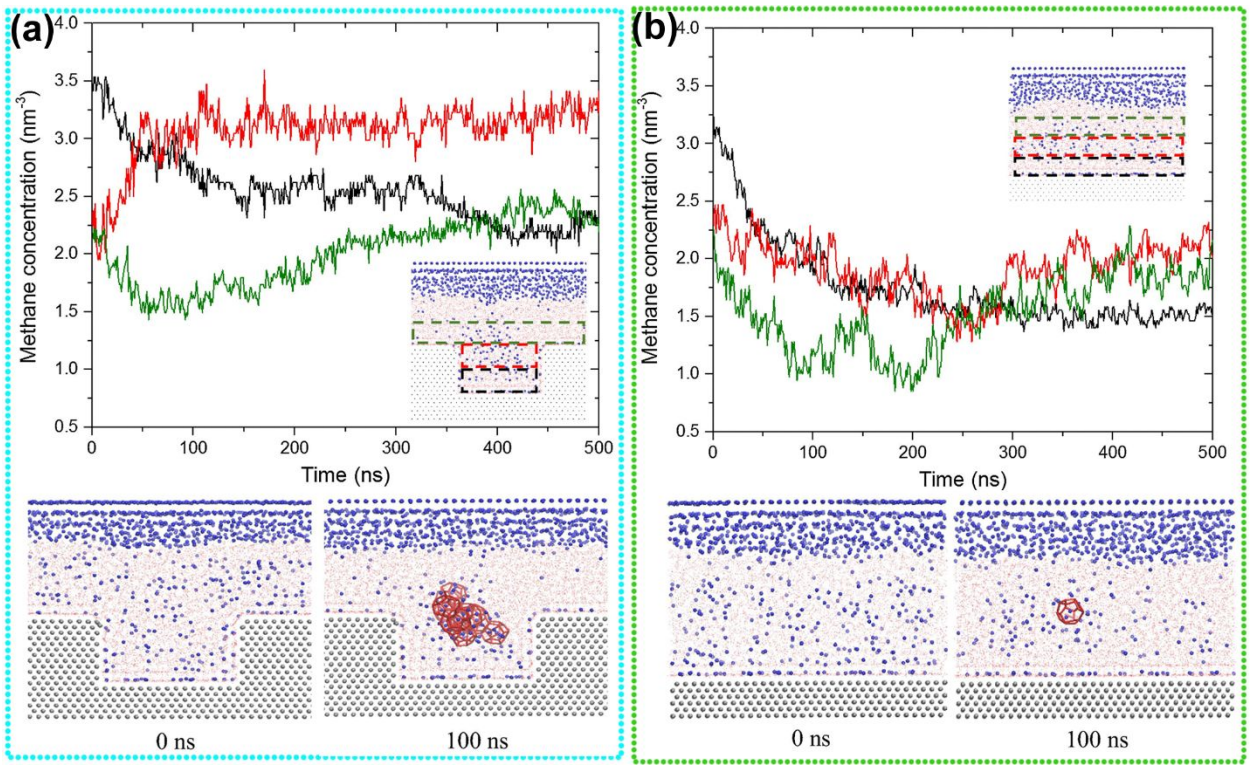

Figure 5. Surface porous structure and hydrate nucleation. (a) Hydrate nucleation behaviors on rough metal surface with water. A nano-scale hydrate "embryo" consisting of multiple cage units was identified in a nano-groove at 100 ns of simulation time. (b) Hydrate-nucleation behavior on smooth metal surface with water. Only single cage structures were observed in the simulations. Panel (a) and (b) were adapted with permission from Ref. 104, Elsevier Publishing Group.

1.3 Routes to anti-hydrate nucleation surfaces

In summary, bearing in mind this immediately preceding discussion above of sections 1.1 & 1.2, three surface properties, i.e., surface chemistry, surface hydrophobicity and surface porous structure, have been found to be of paramount importance to hydrate nucleation. These three surface properties can be taken as the major design parameters for tuning hydrate nucleation, in addition to other parameters, like surface crystallinity, which can also influence hydrate formation[121]. It is clear that the concentration of guest molecules and intermediate water layer at

the surface determines, in large part, the hydrate-nucleation rate (although one must also bear in mind local supersaturation chemical-potential driving forces and gas-transport limitations, whether through hydrate nano-films or indeed the liquid phase itself) - no matter whether considering hydrate promotion or in inhibition[79, 80, 121-123]. As heterogenous hydrate-nucleation mechanisms have been verified, to a large degree, by molecular simulation in recent years [75, 76, 79, 80, 84, 114], a higher concentration of solvated gas molecules away from surfaces can promote hydrate nucleation, whilst the intermediate ordered water layer near surfaces could stabilize the incipient hydrate crystal and enhance hydrate growth. To design anti-hydrate surfaces which inhibit hydrate nucleation, the promoting effects seen in simulations should be eliminated either through surface-chemistry or surface-hydrophobicity modification. Furthermore, surface roughness and pores structures should be avoided unless oil can be trapped in the grooves or pores for excluding gas molecules. Other surface strategies in controlling gas hydrate nucleation, such as tuning coating flexibility, integrating non-ice binding components or faces onto surface, programming surface barriers for avoiding gas absorption, and embedding kinetic hydrate inhibitors, are amongst the most promising "passive" hydrate mitigation methods, and indeed justify more exploration[103, 112].

2 Anti-hydrate deposition surfaces

Hydrate deposition on pipeline wall is another critical issue in hydrate-plug formation. The factors that determine hydrate deposition include the degree of subcooling, wall heat flux, internal cooling, flow rate, fluid properties and emulsification of liquid phases, and condensation profile[124]. The detailed roles of pipeline surfaces in hydrate deposition are currently not fully understood, although work by Kvamme *et al.* has contributed to initial establishment of this understanding[118, 119]. However, there are important connections between the interactions between hydrates and

surfaces and the hydrate-deposition process[125, 126]. Hence, advanced surfaces design can provide alternative solutions for hydrate deposition.

2.1 Hydrate-deposition mechanisms

Hydrate deposition is commonly observed along with hydrate formation, which can be considered as the intermediate state between hydrate nucleation and hydrate plugging. For a long time, a detailed understanding of hydrate deposition was sorely lacking by the community. Lingelem *et al.* carried out series of promising experiments in 1984 to 1990 for investigating hydrate deposition in pipes[124]. Although the purpose was to illustrate basic mechanisms of hydrate deposition, the lack of precisely controlled experimental systems and limited knowledge on crystal initiation and growth made it difficult to interpret the observations at that time. Despite the progress made in recent decades on "deciphering" hydrate-nucleation and -growth mechanisms in pipelines[127-129], the hydrate-deposition mechanism is still under debate, owing to the difficulty in decoupling hydrate deposition from other hydrate related phenomena (e.g., agglomeration)[130]. Nevertheless, the important role of hydrate deposition in pipelines' plugging is well recognized, because the large pressure drops observed in transport line in hydrate formation cannot be solely resulted by agglomeration of hydrate particles[131]. As early as in 2008, Nicholas *et al.* found that hydrates formed in the bulk phase were not likely to deposit onto pipe wall given the weak adhesion force between "dry" hydrates (without a free water phase) and surfaces[67]. They proposed a hydrate wall-growth model in the same period[68]. Followed up to research efforts on hydrate deposition in various flow systems[131-135], the first hydrate-deposition mechanism was not proposed until 2014, by Grasso *et al.*[130]. There are two suggested potential mechanisms of hydrate deposition in multiphase flow based on experimental observations: hydrate deposition is either caused by

hydrate film growth from a water layer on pipe walls or caused by hydrate particles accumulated on a hydrate base layer due to the cohesive forces between the particles. The hydrate deposition that initiates directly from the closest gas layer on surfaces is possible in theory; however, this has not yet been observed.

Here, in this present review, three mechanisms are summarized based on the current fundamental understanding of hydrate deposition (both physically and chemically), as shown in Fig. 6. Mechanism Ⅰ postulates that a hydrate layer growth on the pipe wall from a surface water layer. This mechanism can explain experimental observation of hydrate growth in saturated gas systems (a predominant gaseous phase with small amounts of water)[130, 134, 135]. In such systems, a water layer can be generated on the pipe walls by direct contact, liquid capillarity, or water evaporation/condensation. In the experiments carried out by Grasso *et al.*, it was found that hydrate deposition occurred immediately as water wetted the pipe wall surfaces[130]. Another experiment performed by Rao *et al.* further revealed the detailed process of hydrate deposition. Specifically, four stages of hydrate deposition were identified - namely the first water film condensation, initial hydrate film growth and gradual coverage of the pipe wall surface, quick outward growth of porous hydrates from the pipe wall surface, and finally the annealing of dense porous hydrate structures[134]. The water layer on the pipe walls can serve as medium for enhanced the interactions between the surfaces and hydrate particles. Hence, hydrate particles establishing contact with the wetted surface could deposit onto the surface through a sintering process. Mechanism Ⅱ hypothesizes that hydrate layers growth from a gas layer (concentrated solvated gas layer or gas nanobubble) on the pipe wall. Different from mechanism Ⅰ, deposition following mechanism II is believed to happen in systems with saturated water (characterized by a free and continuous water layer). Although experiments showed hydrate deposits formed in water-dominated systems and caused

large pressure drop[132, 135], it was not until 2018 that Guo *et al.* successfully observed hydrate deposition initiated by gas bubbles on surfaces with the existence of saturated water[136]. As such, mechanisms Ⅰ and Ⅱ both posit that hydrate deposition arises from hydrate formers on pipe walls, despite their occurrence in distinct systems. In contrast, mechanism Ⅲ subscribes to the view that hydrate deposits onto surfaces through a cohesion process between hydrate particles. This cohesion process can be predicted by the "capillary-bridge" theory in hydrate sintering processes[137]. This theory is based on the understanding that there exists a hydrate quasi-liquid layer which is the precondition for building a capillary connection between hydrate particles. The capillary force then holds the particles together and therefore decreases the total free energy of the system. There are three contributing factors to the cohesive force between particles as depicted in Fig. 6 – namely, the pressure difference between the water bridge and bulk phases, the surface tension between hydrate particles and liquids, and the energy associated with the three-phase contact line[137, 138]. The cohesive force can be further predicted according to the report from Zachary *et al.* by considering the bridge-bulk interfacial tension, the contact angle of the bridge on the particles and some measure of the physical dimensions of the capillary bridge[137]. It is worth noting that water-capillary bridges resemble the effect of water layer in mechanism Ⅰ. Given enough time for gas-mass-transport-limited guest diffusion thereto and saturation therein, the water-capillary bridges turned into hydrate, which was a critical step in the hydrate sintering process, and ultimately resulting in catastrophic hydrate plugging of the pipeline.

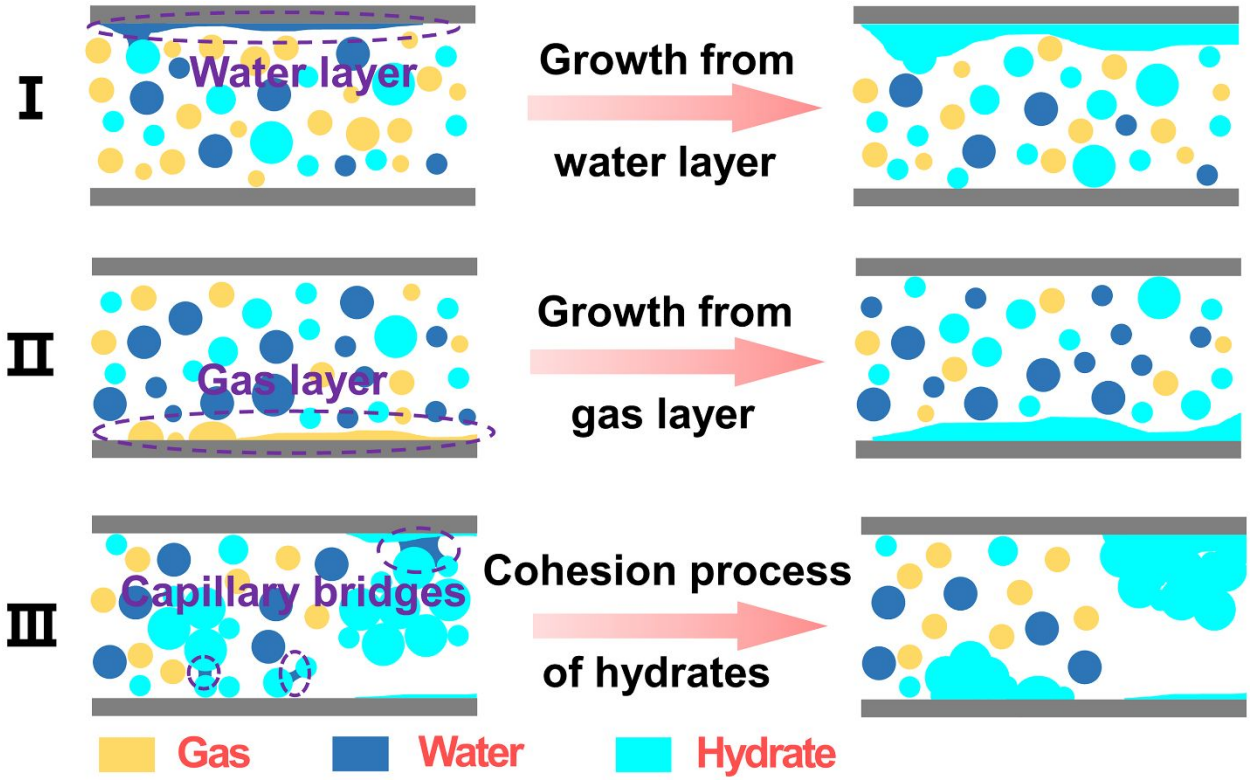

Figure 6. Hydrate-deposition mechanisms. Mechanism Ⅰ and Ⅱ hypothesize a hydrate layer grows on the pipe wall from a surface water layer and a surface gas layer, respectively. Mechanism Ⅲ postulates that hydrate deposition onto surfaces through a cohesion process among hydrate particles.

2.2 Surface property and hydrate deposition

Because the three mechanisms discussed above emphasize that hydrate deposition is initiated by water, gas, and hydrate particles on pipe surfaces, respectively, the interactions between water/gas/hydrate and surfaces are thus key to hydrate deposition. Accordingly, anti-hydrate deposition surfaces have been designed with targets in mind of suppressing water, gas or hydrate particles from accumulating or building on pipe walls in different flow systems. As the schematic picture shows in Fig. 7, five parameters were identified as the essential factors that controlled hydrate deposition - namely the hydrate-formation driving force (temperature and pressure), the amount of adhesive water, the surface property, the surface mass transfer coefficient, and the flow

shear rate[139]. The impacts of surface property on anti-hydrate deposition affected specifically the surface free energy, gas wettability and surface structure, and are detailed below.

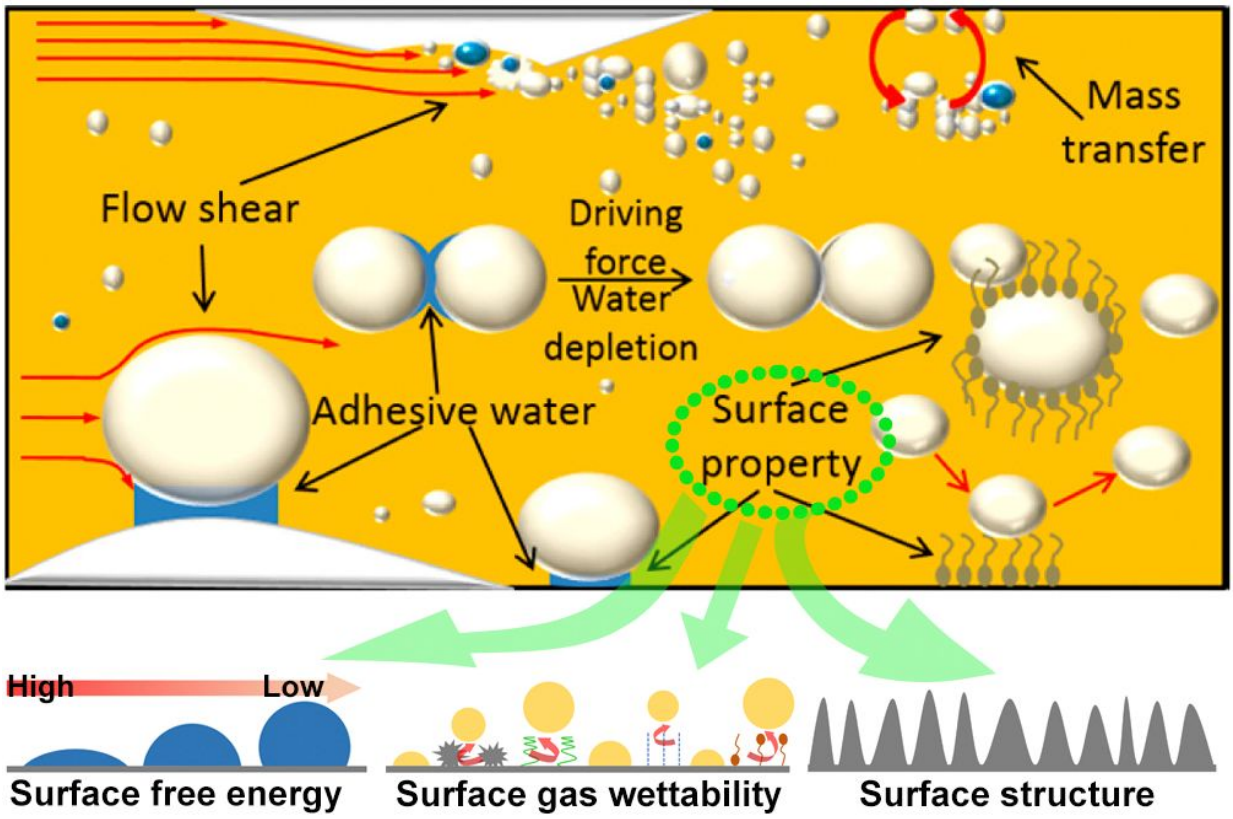

Figure 7. Surface parameters that affect hydrate deposition. Schematic diagram of the influencing factors in hydrate deposition process was adapted with permission from Ref. 139, American Chemical Society. The surface properties considered for anti-hydrate deposition are surface free energy, gas wettability and surface structure.

2.2.1 Surface free energy and hydrate deposition

The free energy of solid surfaces is known to strongly influence wetting, adsorption and adhesion behaviors, and is believed to be of great importance to hydrate deposition[140, 141]. As early as in 1998, Sonin *et al.* investigated water wetting and hydrate formation behavior in water-oil-metal substrate systems, and revealed the connection between surface wettability and hydrate crystallization[108]. Aspenes *et al.* further established the relationship between surface free energy

of pipeline materials and hydrate deposition[141]. As shown in Fig. 8, they utilized five surfaces with various surface free energies, and quantified water adhesion energies on the surfaces in oil environments (petroleum ether). As such, they achieved two important conclusions in their study. Firstly, increases in surface free energy led to increased adhesion energy of water, meaning the surface became more water-wet in oil. Secondly, additives/impurities in oil can affect the adhesion of water on different surfaces. They found that acid molecules absorbed on surfaces decreased water adhesion energy effectively. Specifically, the water-adhesion energies did not always increase with increasing surface free energy when naphthenic acids existed in the system (Fig. 8b). The different behaviors of the surfaces towards the acids were due to different chemical reactions of surfaces to acids. It was suggested that adhesion energy of surfaces with components that had stronger reactivity with acids (aluminum oxide layer in this work) decreased more when acid existed. Therefore, to reduce water adhesion energy, additive components that had strong reactivity with surfaces were recommended. Suggested by the above-mentioned mechanism Ⅰ, one important principle for designing anti-hydrate deposition surface is by eliminating water on surfaces in saturated gas systems. The results by Aspenes *et al.* clearly indicate that the usage of low-energy surfaces could avoid water-wetting and hydrate deposition, because stable water films on pipeline can be suppressed with minimized water adhesion on surfaces. In another study, Aspenes *et al.* observed similar relationship between surfaces free energy and hydrate deposition[142]. They found the surfaces with lowest free energy, representing the most oil-wet property and having lowest adhesion energy to water in crude oil, had the least hydrate deposition. They suggested a potential strategy for anti-hydrate deposition by using surfaces with strong interactions with additives in the fluids, which can result in absorption of the molecules on the surfaces and greatly lower water adhesion energy and reduce hydrate deposition.

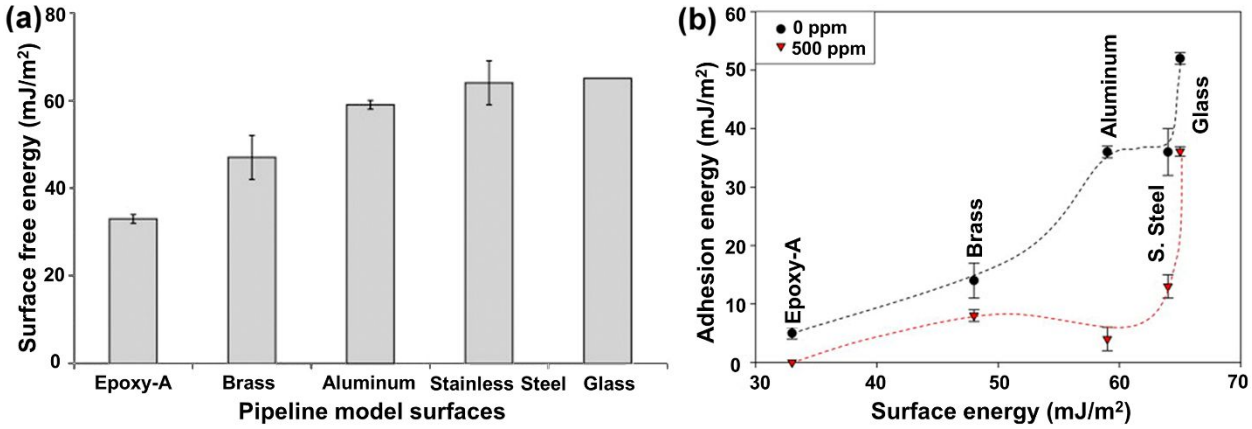

Figure 8. Surface free energy and hydrate deposition. (a) The surfaces with varied free energies used for probing hydrate deposition. (b) The corresponding adhesion energy of brine in oil environment (petroleum ether) on the five surfaces surface in (a) with and without additives of naphthenic acids. Panel (a) and (b) were adapted with permission from Ref. 141, Elsevier Publishing Group.

2.2.2 Surface gas wettability and hydrate deposition

In situations where the surface of the pipe wall is in contact with water-dominated systems, the surface gas-wettability, namely the gas-surface interactions, determines hydrate deposition and underpins anti-hydrate strategies. As discussed in the early sections 1.2 & 1.3 of hydrate nucleation, solid surfaces can provide nucleation sites and initiate hydrate nucleation[85, 87, 143]. Many simulation and experimental results showed that hydrophobic surfaces can promote gas-hydrate formation[144-146]. Recently, it was found that gas enrichment and gas bubbles on hydrophobic surfaces were responsible for the hydrate-nucleation-promotion effects[136, 146, 147]. Therefore, strong surface gas wettability is a significant factor affecting hydrate growth, and, thus, deposition, from gas layers and bubbles on the surfaces. Although surface gas nano-bubbles have been widely observed at the interfaces of water and hydrophobic solid surfaces (which is also known as aerophilic surfaces)[148-152], the relationship between interfacial gas bubbles and hydrate formation have not been established more clearly until 2017. By scrutinizing interfacial layer components on different

surfaces, Nguyen *et al.* pointed out that there was an interfacial-gas enhancement (IGE) effect on hydrophobic surfaces essential promotes hydrate formation[147]. As density profiles of gas and water near hydrophobic and hydrophilic solid surfaces shown in Fig. 9a, and strong enhancements of the gas density of both CH_4 and CO_2 were discovered in the interfacial regions on hydrophobic surfaces, borne in large part by local supersaturation. This gas-enhancement effect was not observed on hydrophilic surfaces, and the gas-density profiles showed opposite trends. In the corresponding experiments, it was found that CO_2 gas bubbles grew more intensively on hydrophobic surfaces - consequently leading to preferential formation of CO_2 gas hydrate on hydrophobic glass surfaces. Although the growth of gas hydrate from gas bubbles was not directly observed, the existence of IGE at hydrophobic interface was found significant in promoting gas hydrate formation. Soon after that, Guo *et al.* reported experimental evidences of methane bubbles on hydrophobic surface as nucleation sites for hydrate formation[136]. In their study, methane hydrate formation was found to be promoted on hydrophobic graphite surfaces, but not so on hydrophilic mica surfaces. As characterized by atomic force microscopy (AFM), a great number of methane nanobubbles with an average diameter ~ 223.4 nm were observed on the graphite surfaces, which was not observed on the mica surfaces. The results led to the following mechanism: methane firstly formed nanobubbles at hydrophobic solid-water interface and then hydrates growth from the bubbles, as indicated by Fig. 9b. Therefore, targeting anti-hydrate deposition following mechanism Ⅱ in saturated water systems, hydrophilic surfaces restraining gas layer at water-surface interfaces are preferred in the design of hydrate-mitigating surfaces.

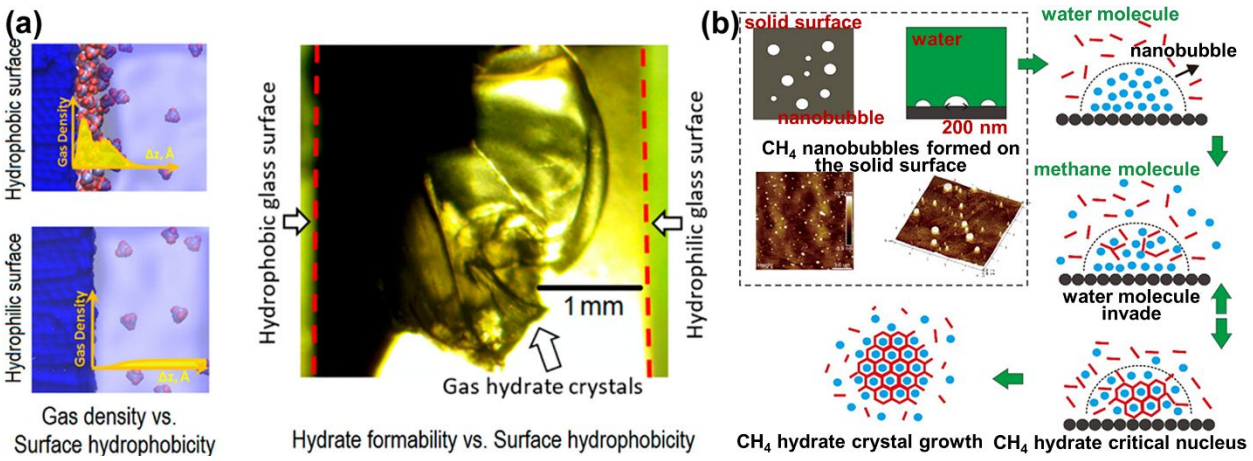

Figure 9. Surface gas wettability and hydrate deposition. (a) Gas-density profiles obtained by simulation and gas hydrate formation in experiments on surfaces with different gas wettability. (b) Evidence of methane nanobubbles formed on hydrophobic surfaces and schematic illustration of gas hydrate growth from a methane nanobubble. Panel (a) and (b) were adapted with permission from Ref. 147 and 136, American Chemical Society.

2.2.3 Surface structure and hydrate deposition

Surface structure affects both surface energy and wettability, and, therefore, strongly influences the behavior of interfacial water, gas and hydrate – all of which adopt critical roles in hydrate deposition. Despite only a few studies devoted on correlating the relationship between surface structure and hydrate deposition, such studies on porous surfaces suggest surface structure could affect hydrate deposition[153, 154]. Specially, Borchardt *et al.* found that methane hydrate formation in confined nanospace were intensified, and Chong *et al.* observed significant amounts of methane hydrate formed atop granular pebble instead of dispersed within the porous media, indicating that porous surfaces can impact hydrate from nucleation to deposition. As has been discussed earlier in the present review on hydrate nucleation part (section 1.2.3), porous structures on surface can significantly influence hydrate nucleation and formation[153-155]. Casco *et al.* have also reported that nanostructures can greatly accelerate methane-hydrate formation in 2015, the confinement effects

of nanostructures enabled faster growth kinetics and lower nucleation pressures while keeping the stoichiometry of methane hydrates[156]. Borchardt *et al.* systematically investigated the effect of pore size on hydrate formation[154], and found that hydrate deposition might be initiated through mechanism Ⅲ once hydrate particles formed on porous surfaces, as shown in Fig. 6. Surface structures can also affect water and gas interaction with surfaces, and, therefore, influences hydrate deposition through mechanisms Ⅰ and Ⅱ. In gas-saturated systems, surface roughness can significantly alter water wettability. As indicated by Wenzel's wetting theory, the water contact angle on a smooth surface θ can be changed by surface structure (with roughness factor *r*) to be θ^* following the relationship $\cos\theta^* = r\cos\theta$[90]. For hydrophilic surfaces ($\theta < 90°$), roughness will enhance water wettability on surfaces. To suppress water layering and subsequent hydrate deposition, roughness on hydrophilic surfaces should be avoided. For hydrophobic surfaces, in contrast, increasing surface roughness can benefit surface-water repellency and enhance anti-hydrate deposition capacity. In water-saturated systems, surface roughness changes the interfacial tension between surfaces and the contacted phase, which should also affect gas-bubble generation and hydrate deposition on the surfaces. Unfortunately, the relationship between surface roughness and gas bubbles' generation in water-saturated systems still awaits in-depth investigation. More efforts are needed to unravel the interaction and stability of gas bubbles on hydrophobic surfaces with different surface structures and elucidating hydrate-deposition mechanisms and behavior.

2.3 Routes to anti-hydrate-deposition surfaces

Based on the current understanding of hydrate-deposition mechanisms and the reported relationships between surface parameters and hydrate deposition, anti-hydrate deposition surfaces, are detailed by design principles, and the corresponding applied flow systems, together with suggested strategies can certainly be proposed, as summarized in Fig. 10. The most crucial step in

inhibition of hydrate deposition lies in suppressing surface precursors, namely either water layer, gas layer or hydrate particles, depending on the system types. To design surfaces that can suppress surface-water layering, surfaces low in free energy are preferred. Hydrophobic surfaces representing low-free-energy surfaces with superior water repellence tend to outperform candidates for gas-dominating systems. Through programming micro/nano structures on hydrophobic surfaces, the water repellence on hydrophobic surfaces can be further enhanced[157], which could be an efficient path for anti-hydrate practices. In contrast, hydrophobic surfaces should be avoided in order to suppress interfacial gas layer in water-saturated systems. The third principle is predicated on suppressing direct hydrate-particle formation on surfaces, and follows the same approach as in eliminating anti-hydrate nucleation, which can be achieved by surface chemistry and physics design. It is important to emphasize that the design of anti-hydrate deposition surfaces should also take the fluids in the pipeline into consideration to a large extent. These surface-design aspects and strategies should be evaluated carefully by analysing the pre-existing flow systems.

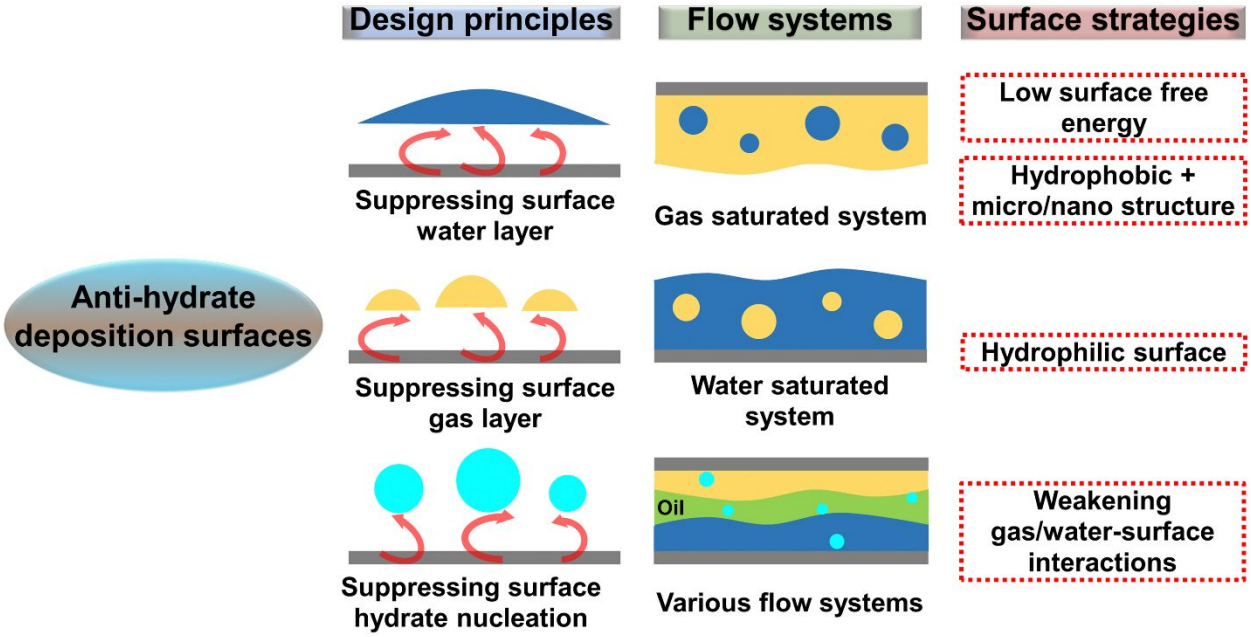

Figure 10. Anti-hydrate deposition surfaces. Design principles are explained as three thematic aspects - suppressing surface-water layering, inhibiting surface-gas layers and mitigating surface hydrate nucleation. The corresponding flow systems and relative surface strategies are also explained.

3 Anti-hydrate adhesion surfaces

In long-distance oil/gas transport pipeline systems, the propensity for hydrate nucleation and deposition under appropriate conditions is by and large inevitable, in practice. Once hydrate films adhere on pipeline walls, either chemical solvents or thermal input are generally required to dissociate hydrates from surfaces[45, 158]. Lowering hydrate-adhesion forces on solid surfaces is thus one plausible, and even rather ideal, anti-hydrate solution[63]. Theoretically, hydrate deposits can be automatically removed by hydrodynamic shear stresses in the pipeline system, given sufficiently low hydrate adhesion strength. In such a way, the resultant hydrate slurry can be transported until it exits the thermodynamically stable region without impeding production. Although hydrate nucleation and formation have been widely investigated[128, 159-162], relatively few studies on hydrate adhesion have been reported, especially for the hydrate-solid adhesion of hydrate growth on surfaces. We shall nonetheless review this limited body of highly relevant work below.

3.1 Hydrate-surface adhesion

Hydrate adhesion on solid surfaces is a complex and multiscale phenomenon. Although the hydrate-solid interactions dominate hydrate-surface adhesion, our understanding of hydrate adhesion varies substantially at different scales. On the nanoscale, hydrate adhesion relies on the intrinsic atomistic interactions between hydrate and surface molecules. Fundamental knowledge on the intrinsic hydrate adhesion can be helpful for identifying the most promising materials (or surface functional groups) that minimize hydrate-surface adhesion. On the microscale, despite

weak adhesion force between "dry" hydrate particle and surface being detected, hydrates can adhere onto surface firmly when the contact time is long enough[67]. This deposition-to-adhesion transition process can be crucial for understanding the key parameters that lead to strong hydrate adhesion. On the continuum scale, it is more feasible for investigating bulk hydrate-solid adhesion given hydrate growth from surface. The hydrate-surface adhesion of this scale is closest to the adhesion of hydrate plugs that adhered on the pipeline, which can be used to estimate the risk of hydrate plugging in practice.

3.1.1 Nanoscale hydrate adhesion

In quantifying hydrate adhesion in most experiments, a micro-mechanical adhesion apparatus was utilized to measure adhesion force between hydrate particles and surfaces[163-165]. Comparing to intrinsic ice adhesion being widely investigated by atomistic modeling and molecular-dynamics simulation in recent years[166-171], intrinsic hydrate adhesion at the atomistic level is, however, largely unexplored. Nevertheless, understanding ice adhesion could nonetheless shed light on the origin of hydrate adhesion, or at least offer some relevant mechanistic hints and parallel insights. Taking atomistic systems constructed for probing nanoscale ice-adhesion mechanisms, as shown in Fig. 11b[166, 167], similar all-atom modeling and molecular-dynamics simulation techniques are highly appropriate for investigating unknown intrinsic hydrate adhesion. For instance, pulling and shearing force can be applied onto nano-sized hydrate structure on different substrates with varied properties, and the resultant hydrate-adhesion mechanics at the nanoscale can be extracted and compared. As such, new atomistic systems of hydrate on solid surface, as shown in Fig. 11b, have been built for exploring hydrate adhesion[172]. By applying a tensile pulling force on hydrate, the detaching stress σ_d was taken as reference of hydrate-adhesion strength, as $\sigma_d = \frac{F_{\max\_pulling}}{A}$

($F_{max\_pulling}$ is the first force peak value in the force profile, A is the hydrate contact area). Given sufficient computing power, surface parameters such as hydrophobicity, roughness, and interfacial lubricant layers can be gauged for their contribution to hydrate adhesion, as the studies performed for ice adhesion[166-171]. It is thus expected that more atomistic modeling and simulations will be carried out for investigating nanoscale hydrate adhesion on surfaces with various properties in the near future. With accumulated results on the nanoscale relationship between hydrate adhesion and surfaces properties, rationalizing atomically-informed anti-hydrate surfaces with low hydrate adhesion could be made more tractable, with the development of "design rules".

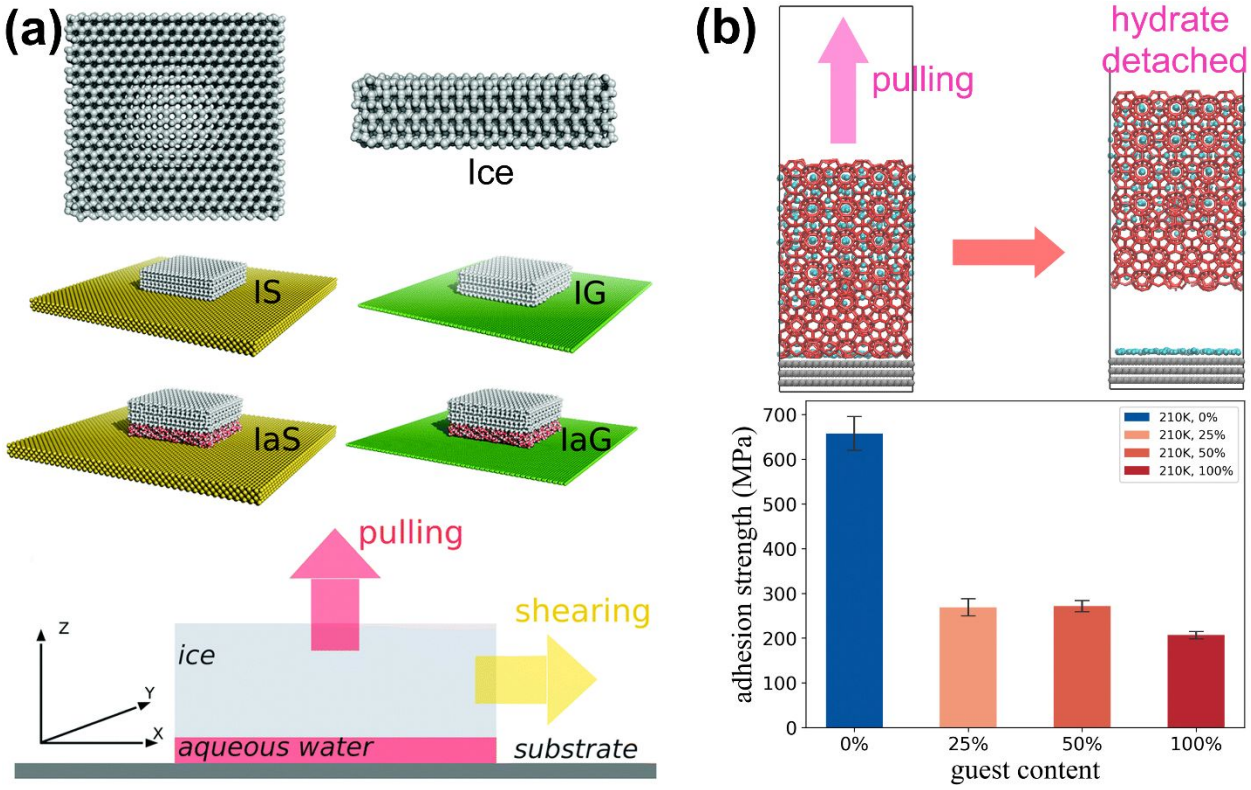

Figure 11. Nanoscale ice and hydrate adhesion. (a) Atomistic models and simulation of ice adhesion on varied solid surfaces. Nanoscale ice cube (top) was built for probing its adhesion strength on different surfaces of hydrophobicity, with and without a lubricant layer of aqueous water. Pulling and shearing force were used in simulations to assess the degree of intrinsic ice adhesion. (b) Simulation systems for investigating nanoscale hydrate adhesion in a recent study. A tensile pulling force was applied to detach hydrate from surfaces and to achieve hydrate adhesion strength. Intrinsic

hydrate adhesion strength on a representative surface with different methane content were compared. Panel (a) was adapted with permission from Ref. 166, Royal Society of Chemistry. Panel (b) was adapted with permission from Ref. 172.

3.1.2 Microscale hydrate adhesion

The microscale adhesion behavior of hydrate particles is commonly investigated by using micromechanical-adhesion testing apparatus[107], as shown in Fig. 12. The determination of hydrate-particle adhesion forces on different surfaces was the focus of most studies[173-176]. To detect the microscale adhesion between hydrate and surfaces, hydrate particles were first brought into direct contacts with or grown directly on a surface of interest, and then removed away from the surface[107, 137, 177]. Nicholas *et al.* systematically investigated the adhesive forces between cyclopentane hydrate and carbon steel by directly contacting the hydrate with the surfaces and holding for approximately 5s under preloaded force[107]. The hydrate adhesive force was calculated using Hooke's law $F = k\delta$, where k is the spring constant of glass fiber holding the hydrate particle and δ is the displacement where hydrate was detached from surface, as shown in Fig. 1a. Their results showed that the adhesive forces between cyclopentane hydrates and carbon steel were substantially lower than hydrate-hydrate adhesive forces, which suggested that the entrained hydrate particles in the flow systems would not deposit on the pipe wall. This work also implied that hydrate deposition was mostly like to form via hydrate growth on the surfaces. As such, it is essential to understand the adhesion strength of hydrates that were grown on the pipe wall. Because there is a quasi-liquid layer at hydrate surfaces[178, 179], this layer can help build capillary bridge between hydrates and solids (as introduced in section 2.1), increasing the holding time of contacting hydrate particles with a surface can trigger a hydrate-sintering process featuring hydrate growth[137]. In such a way, Aman *et al.* systematically investigated the adhesive forces between cyclopentane hydrate

particles and steel surface as a function of contact time[137]. It was found that a threshold waiting time of around 30 s was needed for hydrate sintering to occur. The hydrate adhesion force increased significantly after hydrate growth onto surface. After hydrate sintering and growth for 10 mins, the hydrate adhesion force on the same surface can increase one order of magnitude[177]. Therefore, hydrates that growth on pipe walls are likely to remain adhered thereto under typical prevailing hydrodynamic forces in the pipeline.

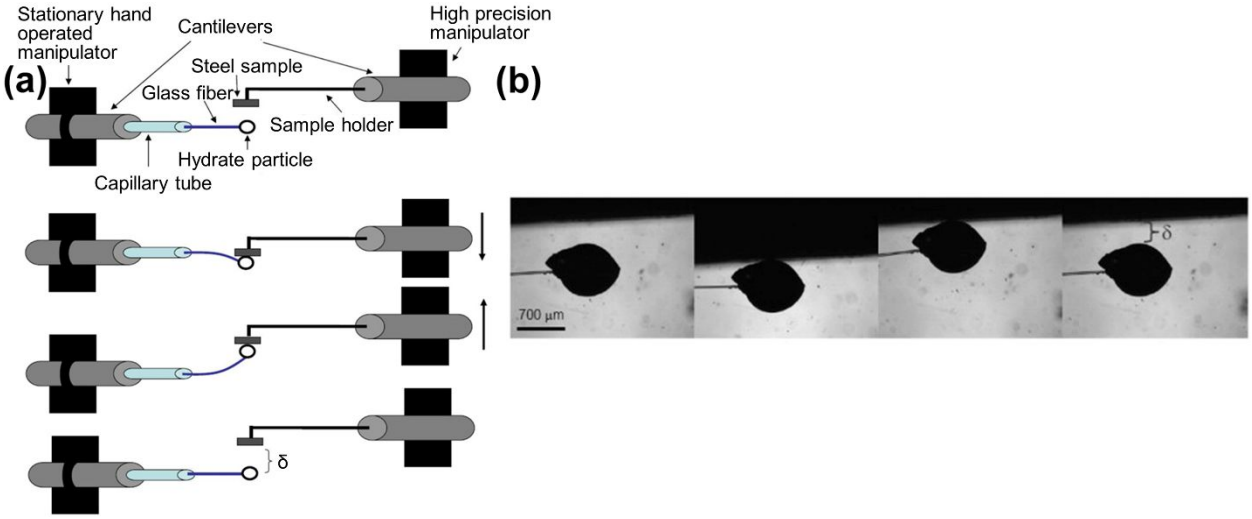

Figure 12. Microscale hydrate adhesion. (a) Schematic of micromechanical adhesion testing apparatus that used for measuring hydrate adhesive force. (b) Example of one measurement using the micromechanical adhesion testing apparatus. Panel (a) and (b) were adapted with permission from Ref. 107, Elsevier Publishing Group.

3.1.3 Continuum-scale hydrate adhesion

The understanding of single hydrate-particle adhesion at the nanoscale could provide insights for anti-hydrate design, especially in the early stages of hydrate deposition. As hydrate accumulate on the pipe wall, continuum-scale studies on hydrate adhesion are highly relevant to hydrate removal in practice. Inspired by studies on continuum-scale ice adhesion, Smith *et al.* introduced a method to measure hydrate-adhesion strength[63], as shown in Fig. 13a. The hydrate adhesion

strength (τ) was quantified through normalizing the maximum probe force (F_{max}) observed in hydrate detachment by the cross-sectional area of hydrate adhesion (A), that is, $\tau = \frac{F_{max}}{A}$. The hydrate adhesion strength was then taken for evaluating surface performances in hydrate removal. According to fracture mechanics, the adhesion strength is correlated with the work of adhesion between two materials[180]. Therefore, one can use the work of adhesion to predict hydrate adhesion on different surfaces. Although the work of adhesion of hydrates to surfaces cannot be easily measured in practice, it can be approximated by quantifying the work of adhesion of a suitable probe fluid with similar surface energy as hydrate. Furthermore, the work of adhesion can also be described using liquid contact angle[181], which eases the task. With theoretical analyses and experimental results, Smith *et al.* proved that there was a close relationship between tetrahydrofuran-hydrate adhesion strength and the receding contact angle of its liquid precursor[63]. Therefore, receding contact-angle measurements provide a practical method for predicting hydrate-adhesion strength and rapid surfaces 'screening' for hydrate-removal capacities. The adhesion strength of hydrate can also be measured through a torsion shear test. The apparatus for torsion shear test was introduced by Lullo *et al.* in 2018 for measuring the adhesion strength of methane hydrate to walls[182]. Although this shearing test for hydrate adhesion has been rarely referred to in the literature, it has provided important information in comparing the shear stress between methane hydrate and tetrahydrofuran hydrate. The results obtained by this setup showed that adhesion strengths of tetrahydrofuran and methane hydrate display distinct differences. Using tetrahydrofuran-hydrate adhesion strength to predict methane-hydrate adhesion strength was inaccurate. Unfortunately, there were not enough samples used in the study to further strengthen the conclusion. More experiments are still needed to clarify the significance of differences in the adhesion of artificial (tetrahydrofuran and cyclopentane hydrate) and methane hydrates. In another

study by Jung *et al.*, hydrate adhesion onto different surfaces were classified using the tensile test, as shown in Fig. 13b[183]. The adhesion behaviors of hydrates made with different guest molecules of CO_2, CH_4 and tetrahydrofuran were investigated. The results showed that adhesion strength of all hydrates can be successfully quantified on mica substrates, but not CO_2 and CH_4 hydrates on calcite. There were failures which occurred in the bodies of CO_2 and CH_4 hydrates on calcite in the experiments. These failures happened when adhesion strength between hydrate and surface stayed beyond cohesive strength of hydrate. The test on smooth mica surfaces always resulted in debonding failure from surfaces for hydrates, and hydrate adhesion strength can be achieved. However, hydrate adhesion strength was not accessible when rougher calcite surfaces were used, because hydrate cohesive failure tended to occur. The study pointed out that the surface properties (including surface roughness and impurities) played essential roles in hydrate-adhesion measurement in experiments. To get convincing and comparable hydrate adhesion strength, adhesive failure of hydrates from surfaces are required.

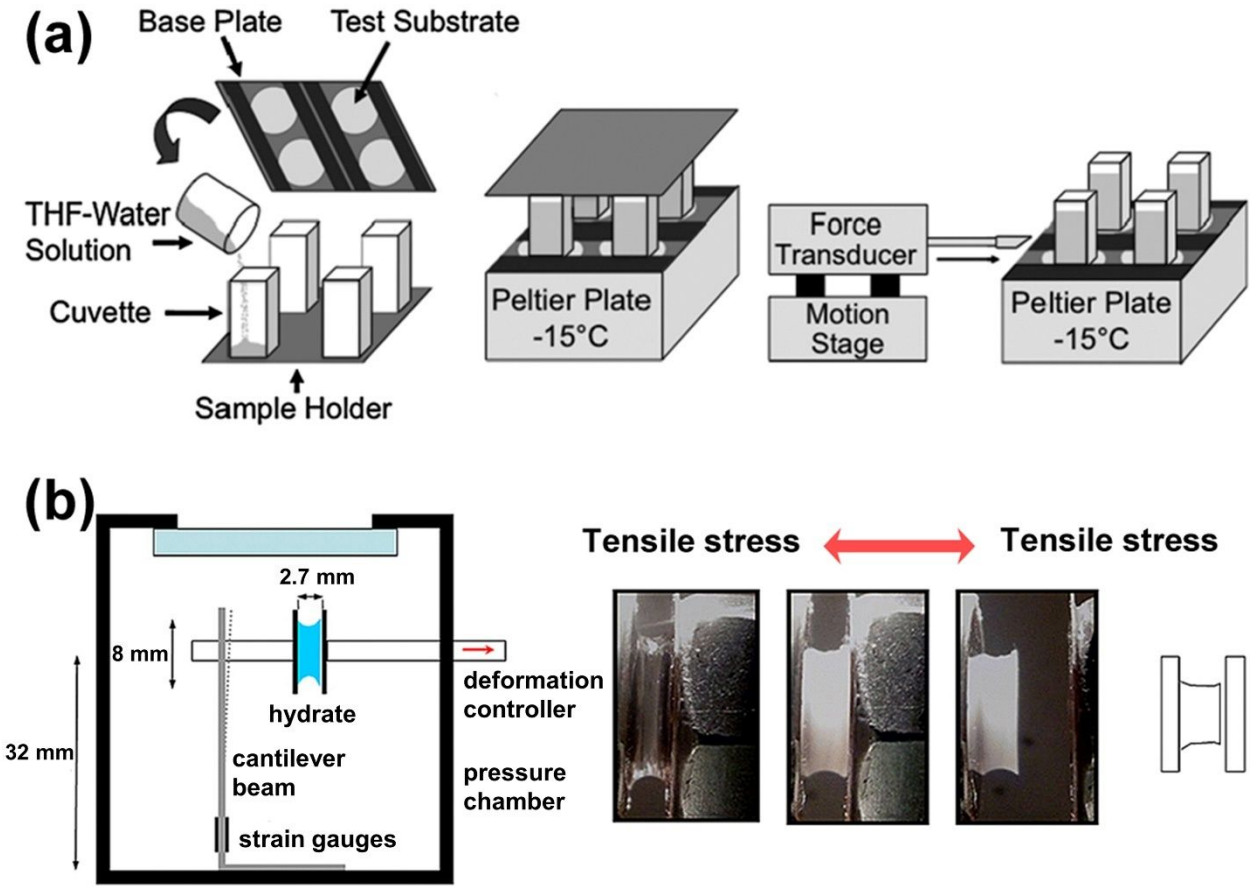

Figure 13. Continuum scale experiments in studying hydrate adhesion. (a) Schematic of the experimental setup 1 and the procedure of freezing hydrate columns on test substrates and measuring the hydrate adhesion strength through shearing test. (b) Schematic of setup 2 and the procedure in probing the hydrate adhesion strength with tensile test. Panel (a) was adapted with from Ref. 63, Royal Society of Chemistry. Panel (b) was adapted with permission from Ref. 183, American Geophysical Union.

3.2 Surface properties and hydrate adhesion

Risk management, rather than total prevention, has been suggested as effective strategies for pipeline hydrate mitigation, meaning allowing hydrates form as long as the hydrates do not lead to plugging[16]. For a long time, the key event that leads to hydrate plugging is believed to be hydrate-particle agglomeration. Therefore, a lot of work has been focused on investigating the adhesion force between hydrate particles and suppressing hydrate agglomeration through

controlling hydrate-hydrate interactions[164, 173-176]. However, more and more studies tend to conclude, correctly, that hydrate deposition and adhesion on solid surfaces play essential roles in plugging[130]. The intrinsic hydrate-solid interactions are of fundamental importance to underlying adhesion mechanism. Because surface properties of pipe walls govern the interactions between hydrate and solid surface, understanding the correlations between surface properties and hydrate adhesion is essential in the design of anti-hydrate surfaces.

3.2.1 Surface free energy and hydrate adhesion

Surface energy is one of the most important properties determining hydrates' adhesion strength. Aspenes *et al.* investigated the adhesion force of cyclopentane hydrate to various surfaces, including glass, stainless steel, carbon steel, aluminum, brass, epoxy coating[177]. The surface free energy was found to be a key parameter affecting hydrate adhesion. As shown in Fig. 14a, the adhesion force between solid and hydrate increased obviously with increasing surface free energy. It is worth noting that hydrate adhesion strength on a continuum scale shows similar trends as a function of surface free energy. Using the method described in Fig. 14a, the hydrate adhesion strength on smooth substrates with various surface energies were systematically and quantitatively studied by Smith *et al.*[63]. The hydrate adhesion strength decreased with decreasing surface free energy, in accordance with similar studies. Moreover, the correlation between hydrate adhesion strength and the practical work of adhesion of a probe fluid with similar surface energy was developed, which provides a firm basis for using liquid receding contact angles as predictor for hydrate adhesion strength (Fig. 14b). However, solely decrease surface free energy for lowering hydrate adhesion was not always applicable. In a study carried out by Das *et al.*, contrasting results were observed[163]. Specifically, silicon surface, silicon surfaces coated with

octadecyltricholorosilane (OTS) and tridecafluoro-1,1,2,2 tetrahydrooctyl-trichlorosilane (FS), with surface energy of ~ 53 mJ m^{-2}, ~ 24 mJ m^{-2} and ~8 mJ m^{-2}, respectively, were subjected to hydrate-adhesion tests. The results showed that the OTS-coated surface had the lowest hydrate adhesion and the most minimized hydrate accumulation atop, which indicated that other parameters might also play important roles on hydrate adhesion.

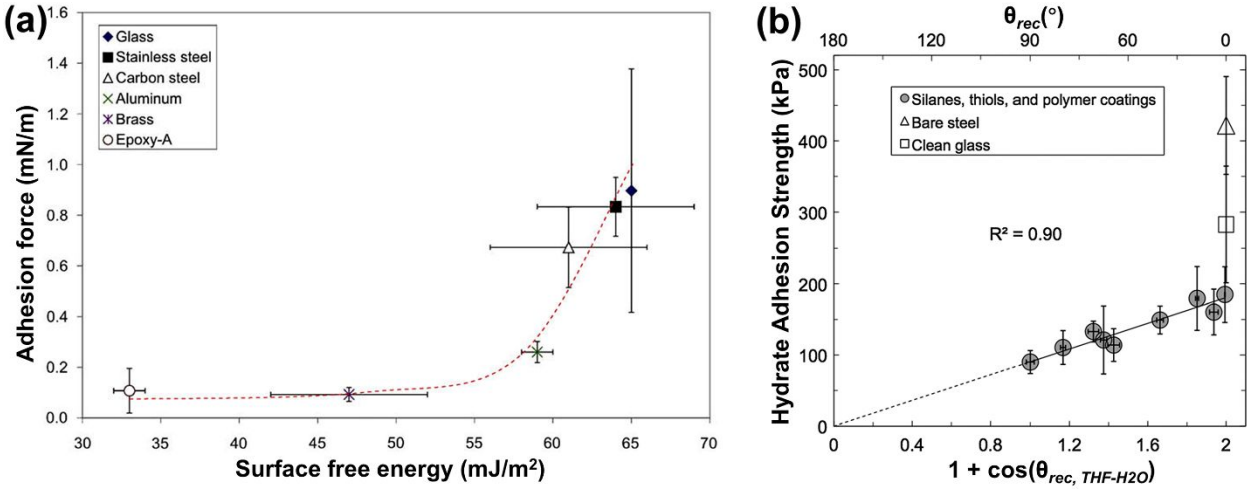

Figure 14. Correlation between surface free energy and hydrate adhesion. (a) Microscale hydrate adhesive force on surfaces with varied surface free energy. (b) Continuum-scale hydrate adhesive force on surfaces with varied surface free energy. Panel (a) was adapted with permission from Ref. 177, Elsevier Publishing Group. Panel (b) was adapted with permission from Ref. 63, Royal Society of Chemistry.

3.2.2 Surface chemistry and hydrate adhesion

There are numerous chemicals with diverse properties included in flow traveling through long-distance pipeline systems for oil/gas transport. Reaction/absorption of these chemicals onto the surfaces of pipe walls can change the surface properties and modify hydrate-surface interactions subsequently. As such, water wettability of the pipe-wall surface can be altered greatly. For instance, naphthenic acids in flow systems can react with pipe-wall materials and change surface-wetting phenomena[141]. Thus, hydrate adhesive force to the surface is also affected by these

chemicals. In microscale adhesion strength tests on various surfaces shown in Fig. 13a, hydrate adhesion forces changed vastly when acids were added into the system. These results suggest that acids in the fluid absorbed onto hydrate surface, solid surface, or both, can reduced the adhesion force between hydrate and surface. The adhesion force was around zero and almost unable to be detected when the flow systems contained 6000 ppm naphthenic acids. Aman *et al.* compared the adhesion forces of cyclopentane hydrate on steel surfaces after modified by different chemicals of oleamide, citric acid ester, nonanedithiol, and Rain-X anti-wetting agent (Rain-X®)[165]. Comparing to the plain steel, oleamide, citric acid ester and Rain-X® surfaces decreased hydrate adhesive forces, although nonanedithiol surface increased this. The increase of hydrate adhesion on nonanedithiol surface was attributed to a rapid hydrate crystal growth at the particle-substrate contact point. The growth began immediately after the hydrate contacted with the substrate, and effectively stabilized hydrate adhesion. Although hydrate growth was also observed on the other surfaces, for instance on surface modified by citric acid ester, the hydrate adhesive forces decreased. The exact mechanism governing the decrease of hydrate adhesion was not yet clear. Nevertheless, the results above clearly illustrated that hydrate adhesion strength on surfaces at the microscale were affected by surfaces' chemical properties in general[184]. The abovementioned studies carried out by Das *et al.* supported such a conclusion[163]. Although the OTS-coated surface had higher surface energy than the FS-coated surface, the hydrate adhesion force on OTS-coated surface was lower. The reason can be explained as the nonpolar $-CH_3$ group on the OTS surface were unfavorable to water, whilst the increased polarity of fluorinated groups on FS surface enhanced the surface-water interactions. Therefore, OTS-coated surface had higher water contact angle, and the hydrate droplet transformed from water can be easily removed from the surface.

3.2.3 Surface-water layer and hydrate adhesion

As discussions above, interfacial water layers on surfaces influence hydrate nucleation as well as deposition. The water layer also significantly affects hydrate adhesion. Correlations between the properties of the water layer and hydrate adhesion has been investigated. In the same work by Aspenes *et al.*, the influence of surface water layer on the adhesion force of cyclopentane hydrate to various surfaces was taken into evaluated (Fig. 15a)[177]. In this study, a water droplet was pre-deposited onto surfaces, followed by hydrate-adhesion measurement (Fig. 15a). Hydrate adhesion force on the wetted surfaces (40 ~ 80 mN/m) underwent a dramatic increase compared to "dry" surfaces (0.1 ~ 1.0 mN/m). In another report by Aman *et al.*, adhesion forces of hydrates on surfaces with different coatings under three wetting conditions were compared[165], as shown in Fig. 15b. Wetted hydrate particles increased hydrate adhesion remarkably, with hydrate adhesive forces increasing by 2-3 orders of magnitude when there was a water layer on surfaces. It is important to note that the influences of surfaces' free energy and surface chemical/physical properties on hydrate adhesion were weakened by water layering in both studies. High adhesive forces were observed on various surfaces with water layers. These results indicate that hydrate can firmly adhere onto pipe walls featuring interfacial water layers on surface. The interfacial water layer is, therefore, one of the most essential parameters in estimating hydrate deposition and adhesion strength on surfaces.

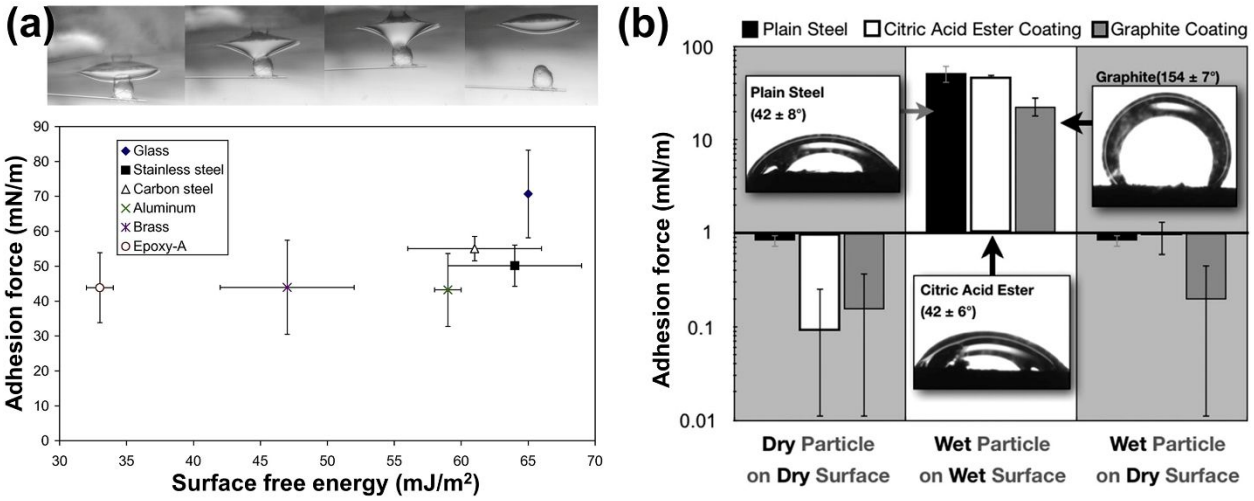

Figure 15. The effect of surface water layer on hydrate adhesion. (a) Microscale hydrate adhesive force of various surfaces with a deposited water droplet. (b) Cyclopentane hydrate adhesive force on uncoated and coated surfaces under three wetting conditions. Panel (a) was adapted with permission from Ref. 177, Elsevier Publishing Group. Panel (b) was adapted with permission from Ref. 165, Royal Society of Chemistry.

3.2.4 Surface roughness and hydrate adhesion

Bearing in mind reported ice-adhesion mechanics, surface roughness can, in principle, have two opposite influences on hydrate adhesion. On the one side, surface roughness can further decrease the contact area of hydrate on surfaces by establishing a Cassie-Baxter wetting state and reduce hydrate adhesion[63, 185, 186]. On the other side, in the case of hydrate forming inside the rough surface structure, mechanical interlocking can lead to enhanced hydrate adhesion[187, 188]. To gain a fundamental understanding on the adhesion of cyclopentane hydrate on rough surfaces, Liu *et al.* measured the adhesion strength of steel substrates polished by 80-, 1000-, and 2000-mesh sandpapers[189]. The surface roughness of samples can be tuned by polishing with different sandpapers. As the results show in Fig. 16a, the monitored hydrate adhesion strength increased significantly with decreased surface roughness. Two reasons were suggested for explaining this trend. Firstly, the rougher structure of steel made it more hydrophilic, and therefore increased the

contact area between the hydrate and the surface. Secondly, the formed hydrate was embedded in the big flaws of the rough surface landscape, and also enhanced the mechanical interactions between the hydrate and the surface. In contrast, the textured structures showed vastly different trends of hydrate adhesion on hydrophobic surfaces. As shown in Fig. 16b, the roughness on two hydrophobic surfaces (OTS-coated and FS-coated surface) were controlled by tuning the distance, *b*, between microposts[163]. For textured FS-coated surfaces, the adhesion force first decreased and then increased with changes in surface roughness. Obviously, increasing the post spacing firstly decreased the contact area between hydrate and surface and decreased the adhesion force. If $b >$ 50 μm, hydrate grew into the roughness structure and increased the adhesion force. Interestingly, the hydrate adhesion force on an OTS-coated surface decreased with increasing post spacing, from 0.02 mN on 5 μm-textured sample to undetectable (< 0.004 mN) on other samples featuring a larger roughness dimension. Overall, surface roughness and roughness parameters on both hydrophilic and hydrophobic surfaces can significantly affect hydrate adhesion.

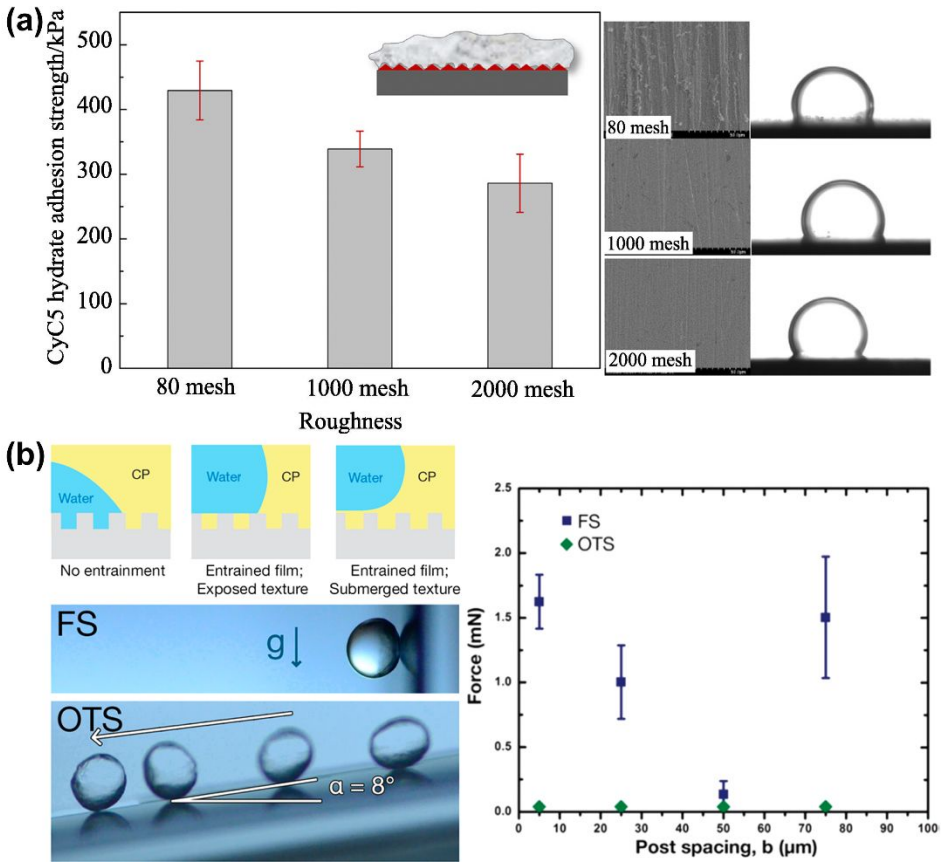

Figure 16. Effect of surface roughness on hydrate adhesion. (a) Hydrate-adhesion strength on steel substrates that polished by various sandpapers, namely with varied roughness dimensions. The contact angles show the water droplets on the steel surfaces in liquid cyclopentane. (b) Thermodynamic states of water on textured surface in cyclopentane and hydrate adhesion force on OTS and FS-treated surfaces with various post spacing. Panel (a) was adapted with permission from Ref. 189, Elsevier Publishing Group. Panel (b) was adapted with permission from Ref. 163, Royal Society of Chemistry.

3.3 Routes to low-hydrate-adhesion surfaces

The fundamental understanding on hydrate adhesion from nano- to continuum-scale, and the current results of the correlations between hydrate adhesion and surface properties, help to shape and inform approaches to low-hydrate-adhesion surface design. The first hydrate-phobic surfaces were reported by McKinley *et al.*, which realized a reduction in hydrate adhesion strength by

roughly 80% (from 422 kPa to 90 kPa) comparing to bare steel surfaces[63]. The low hydrate adhesion was achieved on surfaces characterized by low Lewis acid, Lewis base, and van der Waals interactions, such that the work of adhesion is minimized. McKinley *et al.* also suggested that further reduction at hydrate adhesion might be accessed through tailoring nano-/micro-textured low energy surfaces[63]. As shown in Fig. 17a, utilizing the initiated chemical vapor deposition (iCVD) technology, poly-divinyl benzene (pDVB) and poly(perfl uorodecylacrylate) (pPFDA) bilayer coatings were also designed for lowering hydrate adhesion strength[190-192]. For both tetrahydrofuran and cyclopentane hydrates, the adhesion strength was dramatically decreased on the two coatings thanks to the deposited bilayer polymer films. As shown in Fig. 17a, the tetrahydrofuran hydrate adhesion strength showed around 90% reduction on bilayer surfaces with 40 nm pPFDA from the counterpart bare silicon substrates[190]. Similarly, the silicon substrate coated by bilayer polymer with 10 nm pPFDA resulted in a low cyclopentane hydrate adhesion strength of ~ 22 kPa, which was around 90% reduction comparing to bare silicon substrate (~ 207 kPa)[191]. The adhesion strength on steel substrates before and after polymeric-bilayer coating showed similar trends. Moreover, these polymeric bilayer coatings were also scalable with excellent durability and were mechanically robust, showing the possibility of large-scale production and application. Hydrate-adhesion strength on re-used bilayer coatings showed the same range of values comparing to the newly as-deposited coatings[190, 191]. Furthermore, the hydrate adhesion strength on these bilayer-coated surfaces only increased slightly in four times cycling tests and after 8 hours sand erosion test[192]. In 2017, new surfaces with ultra-low hydrate adhesion surfaces were fabricated by Varanasi *et al.*[163]. The surfaces combined textured structures and low-energy octadecyltricholorosilane modifications. The surface showed super water repellency, therefore creating water-immiscible oil barrier films on top. This oil barrier film drastically

hindered the hydrate-surface interactions, and resulted in facile hydrate removal by negligible force. Recently, Liu *et al.* found that wax coatings can significantly reduce the strength of cyclopentane hydrate adhesion by 95%[193]. By setting quartz sand on the wall, the hydrate-adhesion strength was found to reduce, owing to the decreasing contact area between sintered hydrate and the wall surface. The anti-hydrate performance of superhydrophobic surfaces were also systematically investigated by Fan *et al.* most recently[194, 195]. As shown in Fig. 17b, a significant decrease on hydrate adhesion force was achieved on surface with hydrophobic coatings. In a high-pressure reactor, coated surfaces were found with negligible methane hydrate coverage within the holding time, while bare surfaces were fully covered by hydrate[195]. Another interesting work using magnetic slippery surfaces for lowering hydrate adhesion was newly introduced by Ragunathan *et al.*[196]. The magnetic slippery surfaces had a ferrofluid top layer that consisted of finely dispersed magnetic particles in a carrier fluid. The coating of ferrofluid provided a liquid-liquid interface that can prevent the adhesion of hydrate. With such developments in lowering hydrate-adhesion strength, it is also important to prove that low-hydrate-adhesion surfaces can effectively mitigate hydrate deposition/plugging in pipeline. For such purposes, a superhydrophobic anti-icing coating and an omniphobic corrosion resistant coating were employed by Koh *et al.* to study their effects on hydrate adhesion and deposition on carbon steel surfaces[197]. Both the superhydrophobic and an omniphobic coatings decreased the adhesion force of hydrate particles to surfaces by ~40%. Furthermore, they investigated whether the coating could prevent hydrate deposition on the surfaces using rocking cell tests with 5 vol% water. The omniphobic surface was able to delay hydrate deposition formation for 24 h, with hydrate forming – but, crucially, staying in the bulk without adhering onto the surface. In contrast, the uncoated surface was covered by hydrate deposition and led to plugging within the experimental time, as shown in Fig. 17c. Although all of

the successful surfaces needed to be further verified by practical testing for in-field deployment vis-a-vis anti-hydrate conditions and performance, low-hydrate-adhesion surfaces have indeed demonstrated tremendous potential as outstanding candidate solution in mitigating hydrate-plugging problems.

By summarizing the published results, a successful anti-hydrate surface should have an optimized combination of surface free energy, surface chemistry, and surface texture. The following "design-rule" strategies are suggested by previous studies for achieving low hydrate adhesion - namely lowering surface free energy, embedding chemicals that can decrease interactions between water/hydrate and surface, minimizing surface-water layering, avoiding surface roughness on hydrophilic surface, leveraging surface roughness on hydrophobic surfaces, and, importantly, creating 'barrier' films between water/hydrate and surface. Up to now, the lowest level of hydrate-adhesion strength was achieved on superhydrophobic surfaces, which combined surface textures with low surface energy (Fig. 16b and Fig. 17b)[163, 194, 195, 197, 198]. It is important to emphasize that most published results were observed in microscale adhesion tests of hydrate droplets, which might not hold on macroscale application. As informed by ice adhesion studies on superhydrophobic surfaces, special attention should be paid to the possible catastrophic increase in hydrate adhesion resulting from mechanical interlocking between hydrate and surface structural texture[187, 188, 199, 200]. Furthermore, the degradation of ice-phobicity on superhydrophobic surfaces in cyclic test implies that the durability of superhydrophobic surfaces could also challenge their anti-hydrate performance[201, 202]. Approaches that lower hydrate adhesion strength, and, at the same time, maintaining long-term durability should be adopted in the design of effective anti-hydrate surfaces.

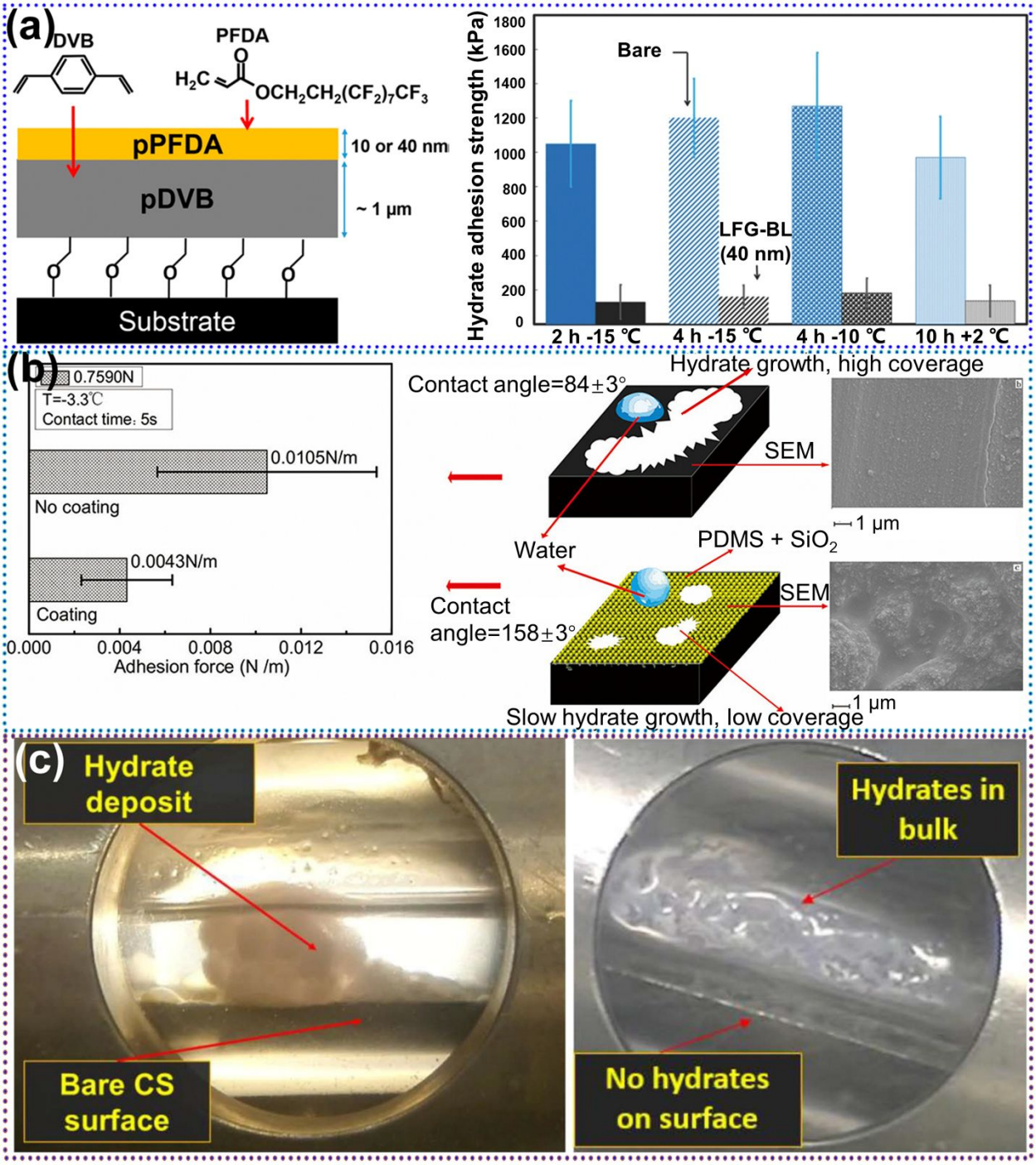

Figure 17. Design of low hydrate adhesion coatings. (a) Schematic illustration of iCVD deposited polymeric bilayer coatings (left) and comparison of tetrahydrofuran hydrate adhesion strength on bare and linker-free grafted bilayer pDVB/pPFDA with a 40-nm-thick pPFDA (LFG-BL (40 nm)) coated silicon substrates (right). (b) The effects of superhydrophobic coatings on reducing hydrate adhesion force and inhibiting hydrate growth. (c) Comparison of

hydrate deposition on the uncoated surface (left) and on the omniphobic surface (right). Low adhesion force between hydrate and omniphobic surface is key to preventing hydrate deposition. Panel (a) was adapted with permission from Ref. 190 and 191, Elsevier Publishing Group. Panel (b) was adapted with permission from Ref. 195, American Chemical Society. Panel (c) was adapted with permission from Ref. 197, Offshore Technology Conference.

4 From anti-icing surfaces to anti-hydrate surfaces

The design of anti-hydrate surfaces can in principle benefit from other relevant research areas. There are numerous studies on surfaces science, such as multi-liquid repellency surfaces, anti-fouling surfaces, and anti-icing surfaces, which provide abundant knowledge for fabricating surfaces to control the accretion of different matter[203-214]. Among these research topics, ice has the most similar properties with hydrate. Hence, the advances in anti-icing surfaces could provide valuable suggestions for future anti-hydrate surfaces design. Generally, state-of-the-art anti-icing surfaces are categorized into surfaces that can repel incoming water droplets, delay ice nucleation, repress ice growth and weaken ice adhesion[215-218]. Inspired by the lotus leaves, many superhydrophobic surfaces are designed for anti-icing purpose. Repelling impacting water before ice nucleation occurs is one of the most popular anti-icing mechanisms, as superhydrophobic surfaces were found to remain entirely ice-free at low temperature down to -25 to -30 °C[215]. Delaying ice nucleation is another common strategy for improving surface repellency to ice. Long term inhibition of ice nucleation has been reported on both superhydrophobic surfaces (~7220 s freezing delay at -10 °C)[219] and graphene coated smooth surfaces (~24000 s freezing delay at -5 °C)[220]. Repressing ice growth is another effective approach for tacking the icing problem, which can be achieved through engineering ice-free zone on surfaces[221-224]. Recently, surfaces with patterned polyelectrolyte were reported to realize large scale ice-free zones (taking up ~ 96% of the entire surface area)[222]. Overall, surfaces using the above three anti-icing strategies can enable

parts of and even the whole surfaces ice free for certain period of time. To prevent hydrate formation on surfaces, the same strategy of repelling surface water for anti-icing is favorite. However, suppressing surface hydrate is much more complex than suppressing surface ice formation due to the co-existence of gas and water under hydrate formation condition. Repelling surfaces gas concentration should also be considered[136]. For instance, superhydrophobic surfaces can be helpful in repelling surface water, while the gas concentrated in the pores can still assist hydrate formation[104]. Therefore, both water and gas wettability need to be evaluated in anti-hydrate surfaces design. Nevertheless, surface strategies that used for delaying ice nucleation and repressing ice growth are rarely corelated with anti-gas hydrate. There are significant possibilities in porting the above knowledge of anti-icing into the design of anti-hydrate surfaces.

In comparison, the principles of anti-icing surfaces design for lowering ice adhesion strength could be highly relevant to anti-gas hydrate surfaces. Because icing is almost unavoidable in natural environment, surfaces with super low ice adhesion that can enable ice removal by wind blow or gravity are desired. Many surfaces have been designed for this purpose, including lubricant infused slippery surface2[225, 226], stress localization surfaces [227], macro-crack initiator surfaces[210, 218], liquid layer generator surfaces[171] and low interfacial toughness (LIT) surfaces[203, 228]. Notably, the recently reported LIT surface is a unique and attractive anti-icing surface. Unlike other icephobic systems that require dramatically high forces for removing ice from large surfaces, the LIT surfaces enable low forces for ice removal independent of interfacial area because its ice delamination relies on the interfacial toughness and not its actual shear strength[203, 228]. The LIT surfaces hence make the scaling-up of anti-icing surfaces possible. The above strategies for low adhesion strength of ice are highly desired in anti-hydrate surfaces design. The interfacial and mechanical mechanisms that used for lowing ice adhesion should also function for anti-hydrate,

considering the similar water-based structure of ice and hydrate. Furthermore, it's also important to consider the dynamic evolution at the hydrate-substrate interfaces after hydrated formed on the surfaces. With the newly reported dynamic anti-icing surfaces, it is known that the ice-solid contact interfaces are not static but rather dynamic in evolution[208]. The dynamic viewpoints are critical for the design of anti-icing surfaces, and likewise to anti-gas hydrate surfaces. Integrating evolving properties that can mitigate the hydrate-solid interactions even after hydrate formed on surfaces can inspire more ideas for future anti-hydrate surfaces design.

Conclusions and perspectives

Although the hydrate-plugging problem has long been known for many years, research into realizing passive anti-gas hydrate surfaces is in its infancy. The current comprehensive review has not only has surveyed all of the relevant studies, but also looks forward to the prospects of a set of coherent "design rules" and criteria to help guide and navigate the development of further novel anti-hydrate surfaces. Surface properties which are important to, and, indeed, underpin, key events in hydrate plugging formation - namely nucleation, growth and agglomeration, deposition, and plugging – have been analyzed and discussed in the present review in some depth. Guiding principles for anti-hydrate surfaces, either targeting anti-hydrate nucleation, anti-hydrate deposition or low hydrate adhesion, can be adopted in surface design for mitigating the hydrate plugging problem. Such a 'blueprinting' picture of novel anti-hydrate surfaces is, however, lacking sufficient "molecular-design" supports from fundamental understandings of hydrate-surface interactions and subsequent hydrate-adhesion mechanics. Currently, building systematic surface strategies for anti-hydrate applications are still challenging.

Firstly, hydrate nucleation, especially heterogenous nucleation, is, to a large extent, determined by surface properties in a complex manner. Although experimental results have suggested that solid surfaces and porous media can greatly affect hydrate formation, their underlying mechanisms remain elusive. Thanks to investigations performed using atomistic modeling simulations, the detailed process of hydrate nucleation can be resolved and systematically analyzed at the atomistic scale. Two main interactions were identified in influencing hydrate nucleation: the interactions between surfaces and guest molecules, and interactions between surfaces and water. On the one hand, surfaces featuring strong interactions with methane will intensify hydrate nucleation on surfaces, as preferential gas-hydrate nucleation always start from regions with higher gas concentration. On the other hand, water-surface interactions can lead to ordered intermediate layers which might stabilize the incipient hydrate crystal and promote hydrate formation. Therefore, strategies that can both weaken gas-surface interactions and water-surface interactions are crucial in the design of anti-hydrate-nucleation surfaces. Despite significant progresses in identifying hydrate nucleation behavior on specific surfaces, systematical analysis and design of surface chemical/physical properties for depressing hydrate nucleation are still absent. Further explorations are in urgent need today.

Secondly, hydrate deposition as an intermediate state between hydrate nucleation and hydrate plugging is also closely affected by surface properties. Unlike hydrate nucleation and adhesion, hydrate-deposition processes are highly diverse in different flow systems, which makes the corresponding design for anti-deposition surfaces extremely difficult. To make it even more complicated, effective ways for anti-hydrate deposition depend on the flow systems, which call for surfaces which can either suppress water deposition, gas deposition or hydrate nucleation. Interestingly, one surface which might have distinct impacts in suppressing surface water and

surface gas - for instance, hydrophobic surfaces - commonly have better water repellence, but can lead to enhanced gas concentration[136, 141, 147]. Consequently, anti-hydrate deposition strategies vary dramatically for different flow systems.

Finally, and more by way of future outlook, hydrate adhesion to solid surfaces depends directly on surface properties. Given that hydrate nucleation and deposition are almost unavoidable in long-distance gas/oil transport systems, building low-hydrate-adhesion surfaces can be the most plausible method for hydrate mitigation. With sufficient low hydrate adhesion to pipe walls, hydrate deposits can be removed under hydrodynamic shear stresses. Some pioneer works have indeed demonstrated prototypes of hydrate-phobic surfaces with low hydrate adhesion. However, rational design of adhesion-suppressant surfaces, or hydrate-phobic surfaces, has been reported very rarely. At the nanoscale, hydrogen boding, van der Waals forces and electrostatic interactions are the major parameters which govern hydrate adhesion strength[218]. Although direct experimental observation of nanoscale hydrate adhesion is still not available, atomistic modeling and simulations can be instead employed for their investigation. The first work on nanoscale hydrate adhesion has been reported recently, as shown in Fig. 11b. Using such a model with atomistic resolution, one can trace the determinants of hydrate-adhesion strength on different surfaces to their intrinsic roots. The obvious advantage of atomistic modeling is the ease of modification on surface properties, such as surface chemistry and roughness, for exploring their direct effects on hydrate adhesion. Given enough computing power, atomistic modeling and simulations can provide key ingredients in formulating candidate anti-hydrate surfaces. On the microscale, hydrate adhesion is affected by interfacial water or oil layers. Water at the contacted area between hydrate and surface can increase the adhesion force between hydrate particles and surfaces. In contrast, the existence of oil at these interfacial regions can prevent direct surface-hydrate interactions, which

lowers hydrate-adhesion strength. Therefore, low-energy surfaces with micro-patterns that can stably trap an interfacial gas/oil layer and maintain Cassie-Baxter state water, or even hydrate atop surfaces, constitute very promising choices[163]. In other words, decreasing the contact area between hydrate and surfaces is an excellent tool in the quest to reduce microscale hydrate adhesion. On the continuum scale, low-ice-adhesion design principles can be borrowed for low hydrate adhesion. It is known that ice adhesion strength (τ_c) is determined by surface parameters, following the relationship $\tau_c = \sqrt{\frac{E^* G}{\pi a \Lambda}}$, where E^* is the Young's modulus of substrate, G is the surface free energy, a is the length of crack generated, and Λ is a non-dimensional constant determined by the geometric configuration of the cracks[188, 218, 225, 229]. Similarly, low-hydrate-adhesion surfaces could be achieved through tuning E^*, G, a, or even Λ. The systematical analyses on low hydrate adhesion from nanoscale to continuum scale can pave the way to realizing passive anti-hydrate surfaces.

In summary, passive anti-gas hydrate surfaces can be realized, at least very much in principle, based on the three guiding, high-level principles discussed above. There are, however, challenges to overcome. First of all, water/gas interactions with surfaces are essential parameters that govern hydrate nucleation and deposition. Surfaces featuring weak interactions with both gas and water are desired for anti-hydrate properties. However, with the experience from reported results, such surfaces either enhance gas concertation or water concentration. A difficult balance between gas-surface and water-surface interactions thus needs to be achieved to progress anti-hydrate surfaces design. Such a balance also applies to anti-hydrate deposition surfaces in various flow systems. Once the environmental conditions of a specific anti-hydrate surface changed, the functionality of the surface could be lost. Another challenge stems from current experiments, both setup and samples, for hydrate adhesion study are, of course, different from real hydrates in pipeline systems. The validity of published results thus can be misleading. Especially, methane-hydrate formation

in pipelines requires both high pressure and low temperature, while model hydrates used in laboratory environments form at normal pressures and artificial temperature. The putative relationship(s), such as they are, between hydrate adhesion strength of model hydrates and methane hydrates are still unknown. Future studies focusing on identifying the correlation between model hydrate and methane hydrate adhesion, or even the correlation between ice and various hydrates adhesion should be carried out. As a closing thought, the durability of anti-hydrate surfaces should be naturally considered in surface design. Improving the surface durability has long been a 'bottleneck' task in the design superhydrophobic and icephobic surfaces, which also apply in anti-hydrate surfaces. The harsh operation conditions in pipelines, corrosion, scaling, rust, and so on, strongly threaten the survival of any anti-hydrate surfaces. It can be foreseen that durability is as important as hydrate-phobicity to hydrate-inhibiting surfaces in practical applications. With the overall systematic discussions on passive anti-gas hydrate surfaces, from suppressing hydrate nucleation, inhibiting hydrate deposition to lowering hydrate adhesion, this review has summarized the challenges needing to be overcome to realize anti-hydrate surfaces. The essential worth of this present work is to inspire novel ideas and lay down key principles in the development of future multifunctional hydrate-phobic surfaces and for their practical applications.

Conflicts of interest

There are no conflicts to declare.

Acknowledgements

The Research Council of Norway is acknowledged for the support to the NANO2021 project Dual-Functional Anti-Gas Hydrate Surfaces (DAndra, 302348) and the support to the FRIPRO project Towards Design of Super-Low Ice Adhesion Surfaces (SLICE, 250990).

References

1. I. U. r. F. Makogon, *Hydrates of natural gas*, PennWell Books Tulsa, Oklahoma, 1981.
2. E. D. Sloan Jr and C. A. Koh, *Clathrate hydrates of natural gases*, CRC press, 2007.
3. A. Vysniauskas and P. Bishnoi, *Chemical Engineering Science*, 1983, **38**, 1061-1072.
4. E. D. Sloan, *Energy & fuels*, 1998, **12**, 191-196.
5. A. Hassanpouryouzband, E. Joonaki, M. V. Farahani, S. Takeya, C. Ruppel, J. Yang, N. J. English, J. M. Schicks, K. Edlmann and H. Mehrabian, *Chemical Society Reviews*, 2020, **49**, 5225-5309.
6. R. K. McMullan and G. Jeffrey, *The Journal of Chemical Physics*, 1965, **42**, 2725-2732.
7. T. C. Mak and R. K. McMullan, *The Journal of Chemical Physics*, 1965, **42**, 2732-2737.
8. J. A. Ripmeester, S. T. John, C. I. Ratcliffe and B. M. Powell, *Nature*, 1987, **325**, 135-136.
9. C. K. Paull, W. Ussler III, W. S. Borowski and F. N. Spiess, *Geology*, 1995, **23**, 89-92.
10. G. Ginsburg, V. Soloviev, R. Cranston, T. Lorenson and K. Kvenvolden, *Geo-Marine Letters*, 1993, **13**, 41-48.
11. Y. Zhu, Y. Zhang, H. Wen, Z. Lu, Z. Jia, Y. Li, Q. LI, C. LIU, P. WANG and X. GUO, *Acta Geologica Sinica-English Edition*, 2010, **84**, 1-10.
12. M. D. Max, *Natural gas hydrate in oceanic and permafrost environments*, Springer Science & Business Media, 2003.
13. J. G. Speight, *Natural gas: a basic handbook*, Gulf Professional Publishing, 2018.
14. E. D. Sloan, *Natural gas hydrates in flow assurance*, Gulf Professional Publishing, 2010.
15. M. A. Kelland, *Energy & fuels*, 2006, **20**, 825-847.
16. E. D. Sloan, *Fluid Phase Equilibria*, 2005, **228**, 67-74.
17. J. Creek, *Energy & Fuels*, 2012, **26**, 4112-4116.
18. C. D. Ruppel and J. D. Kessler, *Reviews of Geophysics*, 2017, **55**, 126-168.
19. R. W. Howarth, *Energy Science & Engineering*, 2014, **2**, 47-60.
20. E. Schulze, S. Luyssaert, P. Ciais, A. Freibauer, I. Janssens, J.-F. Soussana, P. Smith, J. Grace, I. Levin and B. Thiruchittampalam, *Nature Geoscience*, 2009, **2**, 842-850.
21. Z.-g. Sun, R. Wang, R. Ma, K. Guo and S. Fan, *Energy Conversion and Management*, 2003, **44**, 2733-2742.
22. A. Khokhar, J. Gudmundsson and E. Sloan, *Fluid Phase Equilibria*, 1998, **150**, 383-392.
23. H. Ganji, M. Manteghian, M. Omidkhah and H. R. Mofrad, *Fuel*, 2007, **86**, 434-441.
24. Y. H. Mori, *J. Chem. Ind. & Eng. China*, 2003, **54**.
25. P. Babu, P. Linga, R. Kumar and P. Englezos, *Energy*, 2015, **85**, 261-279.
26. A. Eslamimanesh, A. H. Mohammadi, D. Richon, P. Naidoo and D. Ramjugernath, *The Journal of Chemical Thermodynamics*, 2012, **46**, 62-71.
27. H. Tajima, A. Yamasaki and F. Kiyono, *Energy*, 2004, **29**, 1713-1729.
28. Y. Kamata, H. Oyama, W. Shimada, T. Ebinuma, S. Takeya, T. Uchida, J. Nagao and H. Narita, *Japanese journal of applied physics*, 2004, **43**, 362.
29. J. Javanmardi and M. Moshfeghian, *Applied thermal engineering*, 2003, **23**, 845-857.
30. J.-H. Cha and Y. Seol, *ACS Sustainable Chemistry & Engineering*, 2013, **1**, 1218-1224.
31. K.-n. Park, S. Y. Hong, J. W. Lee, K. C. Kang, Y. C. Lee, M.-G. Ha and J. D. Lee, *Desalination*, 2011, **274**, 91-96.
32. K. C. Kang, P. Linga, K.-n. Park, S.-J. Choi and J. D. Lee, *Desalination*, 2014, **353**, 84-90.
33. T. Daitoku and Y. Utaka, *Applied Energy*, 2010, **87**, 2682-2689.
34. X. Wang, F. Zhang and W. Lipiński, *Solar Energy*, 2020, **211**, 11-30.
35. Y. Xie, G. Li, D. Liu, N. Liu, Y. Qi, D. Liang, K. Guo and S. Fan, *Applied energy*, 2010, **87**, 3340-3346.
36. T. Zou, W. Fu, X. Liang, S. Wang, X. Gao, Z. Zhang and Y. Fang, *International Journal of Refrigeration*, 2019, **101**, 117-124.

37. N. H. Duc, F. Chauvy and J.-M. Herri, *Energy Conversion and Management*, 2007, **48**, 1313-1322.
38. H. Dashti, L. Z. Yew and X. Lou, *Journal of Natural Gas Science and Engineering*, 2015, **23**, 195-207.
39. Z. Ma, P. Zhang, H. Bao and S. Deng, *Renewable and Sustainable Energy Reviews*, 2016, **53**, 1273-1302.
40. P. Sun, J. R. Grace, C. J. Lim and E. J. Anthony, *Industrial & Engineering Chemistry Research*, 2008, **47**, 2024-2032.
41. L. Zhang, L. Yang, J. Wang, J. Zhao, H. Dong, M. Yang, Y. Liu and Y. Song, *Chemical Engineering Journal*, 2017, **308**, 40-49.
42. G. Ersland, J. Husebø, A. Graue and B. Kvamme, *Energy Procedia*, 2009, **1**, 3477-3484.
43. B. Kvamme, A. Graue, T. Buanes, T. Kuznetsova and G. Ersland, *International Journal of Greenhouse gas control*, 2007, **1**, 236-246.
44. Y. Lee, S. Lee, J. Lee and Y. Seo, *Chemical Engineering Journal*, 2014, **246**, 20-26.
45. A. K. Sum, C. A. Koh and E. D. Sloan, *Industrial & Engineering Chemistry Research*, 2009, **48**, 7457-7465.
46. B. Kvamme, T. Kuznetsova, J. M. Bauman, S. Sjöblom and A. Avinash Kulkarni, *Journal of Chemical & Engineering Data*, 2016, **61**, 936-949.
47. A. A. Olajire, *Journal of Molecular Liquids*, 2020, 114203.
48. Z. Wang, Y. Zhao, J. Zhang, S. Pan, J. Yu and B. Sun, *Journal of Petroleum Science and Engineering*, 2018, **163**, 211-216.
49. K. K. Østergaard, R. Masoudi, B. Tohidi, A. Danesh and A. C. Todd, *Journal of Petroleum Science and Engineering*, 2005, **48**, 70-80.
50. A. H. S. Dehaghani and M. H. Badizad, *Fluid Phase Equilibria*, 2016, **427**, 328-339.
51. T. Yagasaki, M. Matsumoto and H. Tanaka, *Physical Chemistry Chemical Physics*, 2015, **17**, 32347-32357.
52. H. Tavasoli, F. Feyzi, M. R. Dehghani and F. Alavi, *Journal of Petroleum Science and Engineering*, 2011, **77**, 93-103.
53. M. A. Kelland, *Energy & Fuels*, 2018, **32**, 12001-12012.
54. B. Kvamme, T. Kuznetsova and K. Aasoldsen, *Journal of Molecular Graphics and Modelling*, 2005, **23**, 524-536.
55. M. A. Kelland, T. M. Svartaas, J. Øvsthus and T. Namba, *Annals of the New York Academy of Sciences*, 2000, **912**, 281-293.
56. W. Ke and D. Chen, *Chinese Journal of Chemical Engineering*, 2019, **27**, 2049-2061.
57. M. Rabeony, D. G. Peiffer, C. A. Costello, K. S. Colle, P. J. Wright and L. D. Talley, *Journal*, 2000.
58. C. A. Koh, *Chemical Society Reviews*, 2002, **31**, 157-167.
59. Y.-j. Xu, Y.-l. Zeng, J. Ding and X.-x. YANG, *Natural Gas Industry*, 2007, **27**, 102.
60. C. N. Khalil, N. D. O. Rocha and L. C. F. Leite, *Journal*, 2000.
61. M. De La Fuente, J. Vaunat and H. Marín-Moreno, *Energies*, 2019, **12**, 2178.
62. Y. Bai and Q. Bai, *Subsea engineering handbook*, Gulf Professional Publishing, 2018.
63. J. D. Smith, A. J. Meuler, H. L. Bralower, R. Venkatesan, S. Subramanian, R. E. Cohen, G. H. McKinley and K. K. Varanasi, *Physical Chemistry Chemical Physics*, 2012, **14**, 6013-6020.
64. E. D. Sloan, *Nature*, 2003, **426**, 353-359.
65. Z. M. Aman and C. A. Koh, *Chemical Society Reviews*, 2016, **45**, 1678-1690.
66. D. J. Turner, K. T. Miller and E. D. Sloan, *Chemical Engineering Science*, 2009, **64**, 3996-4004.
67. J. W. Nicholas, L. E. Dieker, C. Koh, E. Sloan, L. Nuelbing, B. Horn and H. He, 2008.
68. J. W. Nicholas, R. R. Inman, J. P. Steele, C. A. Koh and E. D. Sloan, 2008.

69. G. C. Sosso, J. Chen, S. J. Cox, M. Fitzner, P. Pedevilla, A. Zen and A. Michaelides, *Chemical reviews*, 2016, **116**, 7078-7116.
70. J. W. Gibbs, *The collected works of J. Willard Gibbs*, Yale Univ. Press, 1948.
71. E. Sloan Jr and F. Fleyfel, *AIChE Journal*, 1991, **37**, 1281-1292.
72. B. Muller-Bongartz, T. Wildeman and R. Sloan Jr, 1992.
73. R. Radhakrishnan and B. L. Trout, *The Journal of chemical physics*, 2002, **117**, 1786-1796.
74. L. Li, J. Zhong, Y. Yan, J. Zhang, J. Xu, J. S. Francisco and X. C. Zeng, *Proceedings of the National Academy of Sciences*, 2020, **117**, 24701-24708.
75. L. C. Jacobson, W. Hujo and V. Molinero, *Journal of the American Chemical Society*, 2010, **132**, 11806-11811.
76. L. C. Jacobson and V. Molinero, *Journal of the American Chemical Society*, 2011, **133**, 6458-6463.
77. B. Kvamme and M. Clarke, *Energies*, 2021, **14**, 4149.
78. B. C. Knott, V. Molinero, M. F. Doherty and B. Peters, *Journal of the American Chemical Society*, 2012, **134**, 19544-19547.
79. Z. He, K. M. Gupta, P. Linga and J. Jiang, *The Journal of Physical Chemistry C*, 2016, **120**, 25225-25236.
80. M. R. Walsh, G. T. Beckham, C. A. Koh, E. D. Sloan, D. T. Wu and A. K. Sum, *The Journal of Physical Chemistry C*, 2011, **115**, 21241-21248.
81. D. Bai, G. Chen, X. Zhang and W. Wang, *Langmuir*, 2012, **28**, 7730-7736.
82. X. Huang, Z. Li, Y. Deng, W. Cai, L. Gu and H. Lu, *The Journal of Physical Chemistry C*, 2020, **124**, 13966-13975.
83. K. F. Yan, X. S. Li, Z. Y. Chen, Z. M. Xia, C. G. Xu and Z. Q. Zhang, *Langmuir*, 2016, **32**, 7975-7984.
84. Z. J. He, P. Linga and J. W. Jiang, *Langmuir*, 2017, **33**, 11956-11967.
85. K. F. Yan, X. S. Li, Z. Y. Chen, C. G. Xu, Y. Zhang and Z. M. Xia, *Energy & Fuels*, 2018, **32**, 6467-6474.
86. Z. He, J. Zhou, X. Lu and B. Corry, *The Journal of Physical Chemistry C*, 2013, **117**, 11412-11420.
87. S. Cha, H. Ouar, T. Wildeman and E. Sloan, *The Journal of Physical Chemistry*, 1988, **92**, 6492-6494.
88. S. Liang, D. Rozmanov and P. G. Kusalik, *Physical Chemistry Chemical Physics*, 2011, **13**, 19856-19864.
89. T. Young, *Philosophical transactions of the royal society of London*, 1805, 65-87.
90. R. N. Wenzel, *Industrial & Engineering Chemistry*, 1936, **28**, 988-994.
91. A. Cassie and S. Baxter, *Transactions of the Faraday society*, 1944, **40**, 546-551.
92. A. Tuteja, W. Choi, M. Ma, J. M. Mabry, S. A. Mazzella, G. C. Rutledge, G. H. McKinley and R. E. Cohen, *Science*, 2007, **318**, 1618-1622.
93. S. Parvate, P. Dixit and S. Chattopadhyay, *The Journal of Physical Chemistry B*, 2020, **124**, 1323-1360.
94. F. Wang, S. Luo, S. Xiao, W. Zhang, Y. Zhuo, J. He and Z. Zhang, *Journal of hazardous materials*, 2020, **390**, 122176.
95. P. Warrier, M. N. Khan, V. Srivastava, C. M. Maupin and C. A. Koh, *The Journal of chemical physics*, 2016, **145**, 211705.
96. P. Skovborg, H. Ng, P. Rasmussen and U. Mohn, *Chemical Engineering Science*, 1993, **48**, 445-453.
97. D. Kim, Y.-H. Ahn, S.-J. Kim, J. Y. Lee, J. Lee, Y.-j. Seo and H. Lee, *The Journal of Physical Chemistry C*, 2015, **119**, 22148-22153.
98. D. Kim and H. Lee, *Korean journal of chemical engineering*, 2016, **33**, 1977-1988.

99. R. Martos-Villa, S. Guggenheim, M. P. Mata, C. I. Sainz-Díaz and F. Nieto, *American Mineralogist*, 2014, **99**, 401-414.
100. R. T. Cygan, S. Guggenheim and A. F. Koster van Groos, *The Journal of Physical Chemistry B*, 2004, **108**, 15141-15149.
101. S. A. Bagherzadeh, P. Englezos, S. Alavi and J. A. Ripmeester, *Journal of Physical Chemistry B*, 2012, **116**, 3188-3197.
102. S. A. Bagherzadeh, P. Englezos, S. Alavi and J. A. Ripmeester, *The Journal of Physical Chemistry C*, 2012, **116**, 24907-24915.
103. J. R. Hall and P. W. Baures, *Energy & Fuels*, 2017, **31**, 7816-7823.
104. M. C. Zi, D. Y. Chen and G. Z. Wu, *Chemical Engineering Science*, 2018, **191**, 253-261.
105. F. Wang, S. J. Luo, S. F. Fu, Z. Z. Jia, M. Dai, C. S. Wang and R. B. Guo, *Journal of Materials Chemistry A*, 2015, **3**, 8316-8323.
106. Y. Li, M. Chen, H. Z. Song, P. Yuan, D. Liu, B. F. Zhang and H. L. Bu, *Applied Clay Science*, 2020, **186**.
107. J. W. Nicholas, L. E. Dieker, E. D. Sloan and C. A. Koh, *Journal of Colloid and Interface Science*, 2009, **331**, 322-328.
108. A. Sonin, T. Palermo and A. Lubek, *Chemical Engineering Journal*, 1998, **69**, 93-98.
109. M. E. Casco, C. Cuadrado-Collados, M. Martinez-Escandell, F. Rodriguez-Reinoso and J. Silvestre-Albero, *Carbon*, 2017, **123**, 299-301.
110. P. Skovborg and P. Rasmussen, *Chemical Engineering Science*, 1994, **49**, 1131-1143.
111. M. R. Ghaani, C. C. Allen, J. M. Young, P. K. Nandi, S. U. Dandare, T. Skvortsov and N. J. English, *Geomicrobiology Journal*, 2020, **37**, 279-286.
112. M. R. Ghaani, C. C. Allen, T. Skvortsov and N. J. English, *The Journal of Physical Chemistry Letters*, 2020, **11**, 5068-5075.
113. M. R. Ghaani, N. J. English and C. C. Allen, *The Journal of Physical Chemistry Letters*, 2020, **11**, 9079-9085.
114. R. S. DeFever and S. Sarupria, *Journal of Chemical Thermodynamics*, 2018, **117**, 205-213.
115. W. Liu, S. Wang, M. Yang, Y. Song, S. Wang and J. Zhao, *Journal of natural gas science and engineering*, 2015, **24**, 357-364.
116. M. A. Clarke, M. Pooladi-Darvish and P. R. Bishnoi, *Industrial & engineering chemistry research*, 1999, **38**, 2485-2490.
117. B. Li, X.-S. Li and G. Li, *Chemical Engineering Science*, 2014, **105**, 220-230.
118. B. Kvamme, T. Kuznetsova and P.-H. Kivelæ, *Physical Chemistry Chemical Physics*, 2012, **14**, 4410-4424.
119. B. Kvamme and S. A. Aromada, *Journal of Chemical & Engineering Data*, 2017, **62**, 2163-2177.
120. P. Hu, D. Chen, M. Zi and G. Wu, *Fuel*, 2018, **230**, 126-133.
121. D. S. Bai, G. J. Chen, X. R. Zhang, A. K. Sum and W. C. Wang, *Scientific Reports*, 2015, **5**.
122. V. Natarajan, P. Bishnoi and N. Kalogerakis, *Chemical Engineering Science*, 1994, **49**, 2075-2087.
123. Z. He, P. Linga and J. Jiang, *Physical Chemistry Chemical Physics*, 2017, **19**, 15657-15661.
124. M. Lingelem, A. Majeed and E. Stange, *Annals of the New York Academy of Sciences*, 1994, **715**, 75-93.
125. E. P. Brown, D. Turner, G. Grasso and C. A. Koh, *Fuel*, 2020, **264**, 116573.
126. Z. Wang, J. Zhang, B. Sun, L. Chen, Y. Zhao and W. Fu, *Chemical Engineering Science*, 2017, **163**, 145-154.
127. R. L. Christiansen and E. D. Sloan Jr, *Annals of the New York Academy of Sciences*, 1994, **715**, 283-305.
128. M. R. Walsh, C. A. Koh, E. D. Sloan, A. K. Sum and D. T. Wu, *Science*, 2009, **326**, 1095-1098.

129. M. Khurana, Z. Yin and P. Linga, *ACS Sustainable Chemistry & Engineering*, 2017, **5**, 11176-11203.
130. G. A. Grasso, E. D. Sloan, C. Koh, J. Creek and G. Kusinski, 2014.
131. J. W. Lachance, L. D. Talley, D. P. Shatto, D. J. Turner and M. W. Eaton, *Energy & fuels*, 2012, **26**, 4059-4066.
132. J. W. Nicholas, 2008.
133. J. W. Nicholas, C. A. Koh, E. D. Sloan, L. Nuebling, H. He and B. Horn, *AIChE Journal*, 2009, **55**, 1882-1888.
134. I. Rao, C. A. Koh, E. D. Sloan and A. K. Sum, *Industrial & Engineering Chemistry Research*, 2013, **52**, 6262-6269.
135. L. E. Zerpa, Z. M. Aman, S. Joshi, I. Rao, E. D. Sloan, C. Koh and A. Sum, 2012.
136. Y. Guo, W. Xiao, W. Pu, J. Hu, J. Zhao and L. Zhang, *Langmuir*, 2018, **34**, 10181-10186.
137. Z. M. Aman, E. P. Brown, E. D. Sloan, A. K. Sum and C. A. Koh, *Physical Chemistry Chemical Physics*, 2011, **13**, 19796-19806.
138. S. Hu and C. A. Koh, *Langmuir*, 2017, **33**, 11299-11309.
139. L. Ding, B. Shi, J. Wang, Y. Liu, X. Lv, H. Wu, W. Wang, X. Lou and J. Gong, *Energy & Fuels*, 2017, **31**, 8865-8876.
140. F. M. Etzler, *Reviews of Adhesion and Adhesives*, 2013, **1**, 3-45.
141. G. Aspenes, S. Høiland, T. Barth and K. Askvik, *Journal of colloid and interface science*, 2009, **333**, 533-539.
142. G. Aspenes, S. Høiland, A. E. Borgund and T. Barth, *Energy & fuels*, 2010, **24**, 483-491.
143. D. Kashchiev and A. Firoozabadi, *Journal of crystal growth*, 2003, **250**, 499-515.
144. F. Farhang, A. V. Nguyen and K. B. Sewell, *Energy & fuels*, 2014, **28**, 7025-7037.
145. J. Wang, R. Wang, R.-H. Yoon and Y. Seol, *Journal of Chemical & Engineering Data*, 2015, **60**, 383-388.
146. N. N. Nguyen and A. V. Nguyen, *Energy & Fuels*, 2017, **31**, 10311-10323.
147. N. N. Nguyen, A. V. Nguyen, K. M. Steel, L. X. Dang and M. Galib, *Journal of Physical Chemistry C*, 2017, **121**, 3830-3840.
148. P. E. Theodorakis and Z. Che, *Advances in colloid and interface science*, 2019, **272**, 101995.
149. Z. Wu, X. Zhang, X. Zhang, J. Sun, Y. Dong and J. Hu, *Chinese Science Bulletin*, 2007, **52**, 1913-1919.
150. J. W. Tyrrell and P. Attard, *Physical review letters*, 2001, **87**, 176104.
151. X. H. Zhang, A. Quinn and W. A. Ducker, *Langmuir*, 2008, **24**, 4756-4764.
152. M. Cao, Z. Li, H. Ma, H. Geng, C. Yu and L. Jiang, *ACS applied materials & interfaces*, 2018, **10**, 20995-21000.
153. Z. R. Chong, M. Yang, B. C. Khoo and P. Linga, *Industrial & Engineering Chemistry Research*, 2016, **55**, 7981-7991.
154. L. Borchardt, W. Nickel, M. Casco, I. Senkovska, V. Bon, D. Wallacher, N. Grimm, S. Krause and J. Silvestre-Albero, *Physical chemistry chemical physics*, 2016, **18**, 20607-20614.
155. P. Babu, D. Yee, P. Linga, A. Palmer, B. C. Khoo, T. S. Tan and P. Rangsunvigit, *Energy & Fuels*, 2013, **27**, 3364-3372.
156. M. E. Casco, J. Silvestre-Albero, A. J. Ramírez-Cuesta, F. Rey, J. L. Jordá, A. Bansode, A. Urakawa, I. Peral, M. Martínez-Escandell and K. Kaneko, *Nature communications*, 2015, **6**, 1-8.
157. M. Ma and R. M. Hill, *Current opinion in colloid & interface science*, 2006, **11**, 193-202.
158. M. Aminnaji, B. Tohidi, R. Burgass and M. Atilhan, *Journal of Natural Gas Science and Engineering*, 2017, **45**, 840-847.
159. B. J. Anderson, J. W. Tester, G. P. Borghi and B. L. Trout, *Journal of the American Chemical Society*, 2005, **127**, 17852-17862.

160. T. Koga, J. Wong, M. K. Endoh, D. Mahajan, C. Gutt and S. K. Satija, *Langmuir*, 2010, **26**, 4627-4630.
161. P. R. Bishnoi and V. Natarajan, *Fluid phase equilibria*, 1996, **117**, 168-177.
162. D. Kashchiev and A. Firoozabadi, *Journal of crystal growth*, 2002, **243**, 476-489.
163. A. Das, T. A. Farnham, S. Bengaluru Subramanyam and K. K. Varanasi, *ACS Applied Materials & Interfaces*, 2017, **9**, 21496-21502.
164. Z. M. Aman, W. J. Leith, G. A. Grasso, E. D. Sloan, A. K. Sum and C. A. Koh, *Langmuir*, 2013, **29**, 15551-15557.
165. Z. M. Aman, E. D. Sloan, A. K. Sum and C. A. Koh, *Physical Chemistry Chemical Physics*, 2014, **16**, 25121-25128.
166. S. Xiao, J. He and Z. Zhang, *Nanoscale*, 2016, **8**, 14625-14632.
167. S. Xiao, J. He and Z. Zhang, *Acta Mechanica Solida Sinica*, 2017, **30**, 224-226.
168. S. Xiao, B. H. Skallerud, F. Wang, Z. Zhang and J. He, *Nanoscale*, 2019, **11**, 16262-16269.
169. S. Rønneberg, S. Xiao, J. He and Z. Zhang, *Coatings*, 2020, **10**, 379.
170. S. Ringdahl, S. Xiao, J. He and Z. Zhang, *Coatings*, 2021, **11**, 33.
171. F. Wang, S. Xiao, Y. Zhuo, W. Ding, J. He and Z. Zhang, *Materials Horizons*, 2019, **6**, 2063-2072.
172. R. M. F. W. Y. C. S. X. N. E. J. H. Z. Zhang, *Langmuir (In press)*, 2021.
173. C. J. Taylor, L. E. Dieker, K. T. Miller, C. A. Koh and E. D. Sloan Jr, *Journal of colloid and interface science*, 2007, **306**, 255-261.
174. S.-o. Yang, D. M. Kleehammer, Z. Huo, E. D. Sloan and K. T. Miller, *Journal of colloid and interface science*, 2004, **277**, 335-341.
175. L. E. Dieker, Z. M. Aman, N. C. George, A. K. Sum, E. D. Sloan and C. A. Koh, *Energy & Fuels*, 2009, **23**, 5966-5971.
176. C. J. Taylor, L. E. Dieker, K. T. Miller, C. A. Koh and E. D. Sloan, 2008.
177. G. Aspenes, L. Dieker, Z. Aman, S. Høiland, A. Sum, C. Koh and E. Sloan, *Journal of colloid and interface science*, 2010, **343**, 529-536.
178. I. E. Dzyaloshinskii, E. M. Lifshitz and L. P. Pitaevskii, *Advances in Physics*, 1961, **10**, 165-209.
179. D. Nenow and A. Trayanov, *Journal of crystal growth*, 1986, **79**, 801-805.
180. S. Bennett, K. Devries and M. Williams, *International Journal of Fracture*, 1974, **10**, 33-43.
181. D. Bangham and R. Razouk, *Transactions of the Faraday Society*, 1937, **33**, 1459-1463.
182. P. P. Z. Alberto Di Lullo, Alberto Pontarollo, Sebastiano Correra, *Recent Advances in Petrochemical Science* 2018, **4**, 59-61.
183. J. Jung and J. C. Santamarina, *Geochemistry, geophysics, geosystems*, 2011, **12**.
184. W. Lee, S. Baek, J.-D. Kim and J. W. Lee, *Energy & fuels*, 2015, **29**, 4245-4254.
185. D. Quéré, *Annu. Rev. Mater. Res.*, 2008, **38**, 71-99.
186. K. K. Varanasi, T. Deng, J. D. Smith, M. Hsu and N. Bhate, *Applied Physics Letters*, 2010, **97**, 234102.
187. J. Chen, J. Liu, M. He, K. Li, D. Cui, Q. Zhang, X. Zeng, Y. Zhang, J. Wang and Y. Song, *Applied Physics Letters*, 2012, **101**, 111603.
188. M. Nosonovsky and V. Hejazi, *ACS nano*, 2012, **6**, 8488-8491.
189. L. Chenwei, W. Zhiyuan, T. Jinlin, Y. Ci and L. Mingzhong, *Chemical Engineering Science*, 2020, **217**, 115524.
190. H. Sojoudi, M. R. Walsh, K. K. Gleason and G. H. McKinley, *Advanced Materials Interfaces*, 2015, **2**.
191. H. Sojoudi, M. R. Walsh, K. K. Gleason and G. H. McKinley, *Langmuir*, 2015, **31**, 6186-6196.
192. H. Sojoudi, H. Arabnejad, A. Raiyan, S. A. Shirazi, G. H. McKinley and K. K. Gleason, *Soft matter*, 2018, **14**, 3443-3454.

193. C. Liu, X. Zeng, C. Yan, C. Zhou, M. Li and Z. Wang, *Langmuir*, 2020.
194. W. Zhang, S. Fan, Y. Wang, X. Lang and G. Li, *Chemical Engineering Journal*, 2021, 129651.
195. S. Fan, H. Zhang, G. Yang, Y. Wang, G. Li and X. Lang, *Energy & Fuels*, 2020, **34**, 13566-13579.
196. T. Ragunathan, X. Xu, J. A. Shuhili and C. D. Wood, *ACS omega*, 2019, **4**, 15789-15797.
197. E. Brown, S. Hu, S. Wang, J. Wells, M. Nakatsuka, V. Veedu and C. Koh, 2017.
198. S. Dong, M. Li, C. Liu, J. Zhang and G. Chen, *J Bionic Eng*, 2020, **17**, 1019-1028.
199. S. Jung, M. Dorrestijn, D. Raps, A. Das, C. M. Megaridis and D. Poulikakos, *Langmuir*, 2011, **27**, 3059-3066.
200. S. Kulinich, S. Farhadi, K. Nose and X. Du, *Langmuir*, 2011, **27**, 25-29.
201. S. Farhadi, M. Farzaneh and S. Kulinich, *Applied Surface Science*, 2011, **257**, 6264-6269.
202. Y. Wang, J. Xue, Q. Wang, Q. Chen and J. Ding, *ACS applied materials & interfaces*, 2013, **5**, 3370-3381.
203. A. Dhyani, J. Wang, A. K. Halvey, B. Macdonald, G. Mehta and A. Tuteja, *Science*, 2021, **373**, eaba5010.
204. T.-S. Wong, S. H. Kang, S. K. Tang, E. J. Smythe, B. D. Hatton, A. Grinthal and J. Aizenberg, *Nature*, 2011, **477**, 443-447.
205. D. Wang, Q. Sun, M. J. Hokkanen, C. Zhang, F.-Y. Lin, Q. Liu, S.-P. Zhu, T. Zhou, Q. Chang and B. He, *Nature*, 2020, **582**, 55-59.
206. V. B. Damodaran and N. S. Murthy, *Biomaterials research*, 2016, **20**, 1-11.
207. Q. Xie, J. Pan, C. Ma and G. Zhang, *Soft Matter*, 2019, **15**, 1087-1107.
208. F. Wang, Y. Zhuo, Z. He, S. Xiao, J. He and Z. Zhang, *Advanced Science*, 2021, 2101163.
209. Y. Zhuo, J. Chen, S. Xiao, T. Li, F. Wang, J. He and Z. Zhang, *Materials Horizons*, 2021.
210. Z. He, Y. Zhuo, F. Wang, J. He and Z. Zhang, *Progress in Organic Coatings*, 2020, **147**, 105737.
211. Y. Zhuo, S. Xiao, V. Håkonsen, T. Li, F. Wang, J. He and Z. Zhang, *Applied Materials Today*, 2020, **19**, 100542.
212. Y. Zhuo, T. Li, F. Wang, V. Håkonsen, S. Xiao, J. He and Z. Zhang, *Soft Matter*, 2019, **15**, 3607-3611.
213. Z. He, Y. Zhuo, F. Wang, J. He and Z. Zhang, *Soft Matter*, 2019, **15**, 2905-2910.
214. Y. Zhuo, F. Wang, S. Xiao, J. He and Z. Zhang, *ACS omega*, 2018, **3**, 10139-10144.
215. L. Mishchenko, B. Hatton, V. Bahadur, J. A. Taylor, T. Krupenkin and J. Aizenberg, *ACS nano*, 2010, **4**, 7699-7707.
216. P. Tourkine, M. Le Merrer and D. Quéré, *Langmuir*, 2009, **25**, 7214-7216.
217. J. Liu, C. Zhu, K. Liu, Y. Jiang, Y. Song, J. S. Francisco, X. C. Zeng and J. Wang, *Proceedings of the National Academy of Sciences*, 2017, **114**, 11285-11290.
218. Z. He, S. Xiao, H. Gao, J. He and Z. Zhang, *Soft Matter*, 2017, **13**, 6562-6568.
219. P. Guo, Y. Zheng, M. Wen, C. Song, Y. Lin and L. Jiang, *Advanced Materials*, 2012, **24**, 2642-2648.
220. N. Akhtar, G. Anemone, D. Farias and B. Holst, *Carbon*, 2019, **141**, 451-456.
221. Y. Yao, T. Y. Zhao, C. Machado, E. Feldman, N. A. Patankar and K.-C. Park, *Proceedings of the National Academy of Sciences*, 2020, **117**, 6323-6329.
222. Y. Jin, C. Wu, Y. Yang, J. Wu, Z. He and J. Wang, *ACS nano*, 2020, **14**, 5000-5007.
223. A. Kirillova, L. Ionov, I. V. Roisman and A. Synytska, *Chemistry of Materials*, 2016, **28**, 6995-7005.
224. S. F. Ahmadi, S. Nath, G. J. Iliff, B. R. Srijanto, C. P. Collier, P. Yue and J. B. Boreyko, *ACS applied materials & interfaces*, 2018, **10**, 32874-32884.
225. F. Wang, W. Ding, J. He and Z. Zhang, *Chemical Engineering Journal*, 2019, **360**, 243-249.
226. J. Lv, Y. Song, L. Jiang and J. Wang, *ACS nano*, 2014, **8**, 3152-3169.
227. P. Irajizad, A. Al-Bayati, B. Eslami, T. Shafquat, M. Nazari, P. Jafari, V. Kashyap, A. Masoudi, D. Araya and H. Ghasemi, *Materials Horizons*, 2019, **6**, 758-766.

228. K. Golovin, A. Dhyani, M. Thouless and A. Tuteja, *Science*, 2019, **364**, 371-375.
229. H. Yao and H. Gao, *Journal of Computational and Theoretical Nanoscience*, 2010, **7**, 1299-1305.